PHYSICAL REVIEW D **88,** 056012 (2013)

Combining heavy quark spin and local hidden gauge symmetries in the dynamical generation of hidden charm baryons

C. W. Xiao,[1,2] J. Nieves,[2] and E. Oset[1,2]

[1]*Departamento de Física Teórica, Universidad de Valencia, 46071 Valencia, Spain*

[2]*IFIC, Centro Mixto Universidad de Valencia-CSIC, Institutos de Investigación de Paterna, Apartado 22085, 46071 Valencia, Spain*

(Received 24 April 2013; published 13 September 2013)

We present a coupled channel unitary approach to obtain states dynamically generated from the meson-baryon interaction with hidden charm, using constraints of heavy quark spin symmetry. As a basis of states, we use $\bar{D}B$, $\bar{D}^*B$ states, with B baryon charmed states belonging to the 20 representations of SU(4) with $J^P = 1/2^+, 3/2^+$. In addition we also include the $\eta_c N$ and $J/\psi N$ states. The inclusion of these coupled channels is demanded by heavy quark spin symmetry, since in the large m_Q limit the D and D^* states are degenerate and are obtained from each other by means of a spin rotation, under which QCD is invariant. The novelty in the work is that we use dynamics from the extrapolation of the local hidden gauge model to SU(4), and we show that this dynamics fully respects the constraints of heavy quark spin symmetry. With the full space of states demanded by the heavy quark spin symmetry and the dynamics of the local hidden gauge, we look for states dynamically generated and find four basic states that are bound, corresponding to $\bar{D}\Sigma_c$, $\bar{D}\Sigma_c^*$, $\bar{D}^*\Sigma_c$, and $\bar{D}^*\Sigma_c^*$, decaying mostly into $\eta_c N$ and $J/\psi N$. All the states appear in isospin $I = 1/2$, and we find no bound states or resonances in $I = 3/2$. The $\bar{D}\Sigma_c$ state appears in $J = 1/2$ and the $\bar{D}\Sigma_c^*$ in $J = 3/2$; the $\bar{D}^*\Sigma_c$ appears nearly degenerate in $J = 1/2, 3/2$ and the $\bar{D}^*\Sigma_c^*$ appears nearly degenerate in $J = 1/2, 3/2, 5/2$, with the peculiarity that in $J = 5/2$ the state has zero width in the space of states chosen. All the states are bound with about 50 MeV with respect to the corresponding $\bar{D}B$ thresholds, and the width, except for the $J = 5/2$ state, is also of the same order of magnitude. Finally, we discuss the uncertainties stemming from the expected breaking of SU(4) and the heavy quark spin symmetry.

DOI: 10.1103/PhysRevD.88.056012 PACS numbers: 11.80.Gw, 12.38.Gc, 12.39.Fe, 13.75.Lb

I. INTRODUCTION

In this paper we investigate hidden charm baryons that come from the interaction of mesons with baryons, with the system containing a $c\bar{c}$ component. This can come from pseudoscalar-baryon or vector-baryon interactions. In [1,2] this problem was faced and, mostly by means of the $\bar{D}\Sigma_c$, $\bar{D}\Lambda_c$ and $\bar{D}^*\Sigma_c$, $\bar{D}^*\Lambda_c$ components, a series of meson-baryon dynamically generated, relatively narrow N^* and Λ^* resonances were predicted around 4.3 GeV. The interaction used in [1,2] was obtained from an extrapolation to SU(4), conveniently broken, of the local hidden gauge dynamics used for SU(3) [3–5].

The local hidden gauge model is dynamically very rich and is considered a good representation of QCD at low energies. In the pseudoscalar sector it contains the lowest order chiral Lagrangian [6,7] and, in addition, the hidden gauge Lagrangian provides the interaction between vectors and their coupling to pseudoscalars. It implements the vector-meson dominance hypothesis of Sakurai [8] and, within this assumption, it also provides the second order Lagrangian for the pseudoscalar-pseudoscalar interaction of [7], as shown in [9]. The use of the local hidden gauge Lagrangian in connection with coupled channels and unitary techniques provides a tool that allows one to study vector-meson interactions in the intermediate energy range where the interaction itself gives rise to dynamically generated states. This is the case for the $\rho\rho$ interaction, from where one obtains the $f_2(1270)$ and $f_0(1370)$ resonances [10] and the extension to the interactions of vectors of the ρ nonet [11], where a few more dynamically generated resonances are obtained, like the $f_0(1710)$, $f_2'(1525)$, and $K_2^*(1430)$. The properties of the resonances obtained are shown to be consistent with the radiative decay to two photons [12] and to two-photon and one-photon–one-vector mesons in [13]. Similarly, consistency with experiment has been shown in $J/\psi \to \phi(\omega)R$ [14], with R being any of the resonances of [11], and in J/ψ radiative decays in [15]. The extension of these ideas to the charm and hidden charm sectors has also shown that some of the excited D states and X, Y, Z states recently reported could be explained in terms of molecules involving mesons with charm [16–22].

The extension of the local hidden gauge approach to the baryon sector for the interaction of vector mesons with baryons has also been tackled: the interaction of vector mesons with the decuplet of baryons is studied in [23] and with the octet of baryons in [24]. In both cases some dynamically generated resonances are obtained that can be associated with resonances reported by the PDG [25]. One step forward in this direction is the consideration of a vector baryon and a pseudoscalar baryon simultaneously in the interaction, which has been done in [26]. A thorough work in this direction has also been done in [27–29]. A review of the hidden gauge approach for vector-baryon and vector-nucleus interactions can be seen in [30].

Work in the charm sector for meson-baryon interactions has been done along different lines, sharing similarities with the local hidden gauge approach [31–34]. A different approach is done in [35], where one uses an analogy of the work for the $\bar{K}N$ interaction and replaces an s quark by a c quark. As mentioned in [36], while the potentials obtained are fine with this prescription, some coupled channels, that mix charm and strangeness, are missing in that approach. In [36,37] the work of [31] is retaken and appropriate modifications are done in the potentials and the regularization scheme. Similar work is also done by the Jülich group in [38–40]. All these works share the dynamical generation of the $\Lambda_c(2595)$, which comes mostly from the interaction of the DN channel. Some hidden charm baryonic states are also generated in [33], albeit with a binding of the order of 1000 MeV, which is difficult to accommodate with the generated potentials, as discussed in [1,2].

As we can see, the topic of baryonic molecules with charm and hidden charm has attracted much attention, and the upcoming FAIR facility is certainly stimulating much work along these lines. Yet, an element missing, in principle, in these works is the consideration of heavy quark spin symmetry (HQSS), which should be a good symmetry when working with mesons and baryons with charm. From the point of view of HQSS, which is a proper QCD spin-flavor symmetry [41–43] when the quark masses become much larger than the typical confinement scale, $\Lambda_{\rm QCD}$, one should consider, in the same footing, D and D^* as well as charmed members of the 20 SU(4) representation of baryons containing the octet of the proton and the 20 representation containing the decuplet of the Δ when their isospin and strange contents are the same. Work along these lines was done in [44–47]. In these references, an extended Weinberg-Tomozawa (WT) interaction to four flavors was derived. The model for four flavors includes all basic hadrons (pseudoscalar and vector mesons, and $\frac{1}{2}^+$ and $\frac{3}{2}^+$ baryons); it reduces to the WT interaction in the sector where Goldstone bosons are involved, while it incorporates HQSS in the sector where charm quarks participate. Charmed and strange baryons are studied in [46], where, among other results, a heavy quark spin symmetry doublet is associated with the three stars $\Xi_c(2790)$ and $\Xi_c(2815)$ pair of resonances. Moreover, the model derived in Ref. [46] also naturally accommodates the three-star charmed resonances $\Lambda_c(2595)$ and $\Lambda_c(2625)$. The $\Lambda_c(2595)$ was previously dynamically generated in other schemes based on t-channel vector-meson-exchange models [33,35–37], but in [46], as first pointed out in [44], a large (dominant) ND^* component in its structure was claimed. This is in sharp contrast to the findings of the former references, where it was generated mostly as one ND bound state since the ND^* channel was not considered in the coupled channels space. The work of Ref. [48] takes advantage of the underlying spin-flavor extended WT structure of the couplings of the model of Refs. [44,46], and it is used to study odd-parity bottom-flavored baryon resonances by replacing a c quark by a b quark.[1] Two resonances, $\Lambda_b(5912)$ and $\Lambda_b(5920)$, which are heavy quark spin symmetry partners, are predicted in [48] and turn out to be in excellent agreement with the two narrow bottom baryon resonances recently observed by the LHCb Collaboration [49]. Finally, in [47] the model of Ref. [46] is extended to the hidden charm sector, the subject of the current work. Seven odd-parity N-like and three Δ-like states with masses around 4 GeV, most of them as bound states, are predicted in [47]. These states form heavy quark spin multiplets, which are almost degenerate in mass. However, the HQSS does not determine the potential; it simply puts some constraints in it. Thus, the determination in the works of [44–48] is made assuming extra elements of SU(8) spin-isospin symmetry. As we will discuss below, here we extend the hidden gauge approach, and the predictions found in this work differ from those obtained in [46] (we do not obtain any isospin $3/2$ states, and the isospin $1/2$ states are significantly heavier, in the region of 4.4 GeV). Besides the use of different dynamics, which are both consistent, as we shall see, with the leading order HQSS requirements, the scheme to renormalize the Bethe-Salpeter equation employed here is also quite different from that advocated in [47], which, for the case of the hidden charm sector, leads to appreciable differences. We will give some more details when our results are presented.

The work with baryons along these lines has run parallel to work in the meson sector [50–54]. In these works, an effective field theory that implements leading order (LO) HQSS constraints is constructed, and its consequences are derived. The scheme, however, relies neither on SU(4) flavor symmetry nor on spin symmetry in the light sector. Many dynamically generated resonances are obtained as HQSS partners of the $X(3872)$, $Z_b(10610)$, and $Z_b(10650)$, some of which can be associated with known resonances, but most are predictions.

In the present work, we come back to the local hidden gauge approach and introduce D^* and the members of the 20-plet of the Δ, as demanded by HQSS, but the dynamics linking the different pseudoscalar-baryon and vector-baryon states is taken from the hidden gauge approach. We look again at the hidden charm baryon sector. What we find in this work is that the matrix elements obtained with the dynamics of the local hidden gauge approach respect the HQSS for the dominant terms in the mass of the heavy quarks, something that was not known before. Another finding is that, within this model, the transition from D to D^* states is subleading in the heavy quark mass counting, as is the

[1]The universality of the interactions of heavy quarks, regardless of their concrete (large) mass, flavor, and spin state, follows from QCD [41–43].

transition from the $1/2^+$ baryons of the 20 representation to those of the $3/2^+$ 20 representation. In this sense, the findings of the present work give extra support to earlier works using the local hidden gauge approach where the different spaces were not allowed to connect. Yet, in addition to the states obtained in [1,2] from $DB_{1/2^+}$ and $D^*B_{1/2^+}$, one obtains extra states from the $DB_{3/2^+}$ and $D^*B_{3/2^+}$, which will be reported here.

We also devote a section to evaluating uncertainties tied to the flavor SU(4) symmetry and HQSS breaking, or the regularization of the loops. We show that all of them induce uncertainties on the binding, but the existence of the bound states and the order of magnitude of the binding are quite stable results.

II. LOWEST ORDER HQSS CONSTRAINTS

HQSS predicts that all types of spin interactions vanish for infinitely massive quarks: The dynamics is unchanged under arbitrary transformations of the spin of the heavy quark (Q). The spin-dependent interactions are proportional to the chromomagnetic moment of the heavy quark, and hence they are of the order of $1/m_Q$. The total angular momentum $\vec{J}$ of the hadron is always a conserved quantity, but in this case the spin of the heavy quark $\vec{S}_Q$ is also conserved in the $m_Q \to \infty$ limit. Consequently, the spin of the light degrees of freedom $\vec{S}_l = \vec{J} - \vec{S}_Q$ is a conserved quantity in that limit. Thus, heavy hadrons come in doublets (unless $s_l = 0$), containing states with total spin $j_\pm = s_l \pm 1/2$ [with $\vec{S}_l^2 = s_l(s_l+1)$ and $J^2 = j(j+1)$] obtained by combining the spin of the light degrees of freedom with the spin of the heavy quark $s_Q = 1/2$. These doublets are degenerate in the $m_Q \to \infty$ limit. This is the case for the ground-state mesons D and D^* or D_s and D_s^* which are composed of a charm quark with $s_Q = 1/2$ and light degrees of freedom with $s_l = 1/2$, forming a multiplet of negative-parity hadrons with spins 0 and 1. The entire multiplet of degenerate states should be treated in any HQSS inspired formalism as a single field that transforms linearly under the heavy quark symmetries [42,43]. For finite charm quark mass, the pseudoscalar and vector D meson masses differ by about one pion mass [actually one has $m_D - m_{D^*} = \mathcal{O}(1/(m_D + m_{D^*}))$], and even less for the strange charmed mesons; thus, it is reasonable to expect that the coupling $DN \to D^*N$ might play an important role. This is indeed what happens when SU(8) symmetry is used [44,46]. Conversely, we shall see that with the local hidden gauge dynamics, the transition $DN \to D^*N$, which is mediated by pion exchange, is rather small and vanishes formally in the limit of zero difference between the mass of the D and the D^*. Something similar occurs with the transition from the $1/2^+$ baryons to those with $3/2^+$. As a consequence, four diagonal blocks develop when the hidden gauge dynamics is used, while at the same time the relations due to heavy quark symmetry are exactly fulfilled in each of the blocks. With a different dynamics than the one provided by the SU(8) symmetry, the numerical results that we obtain are also different from those obtained in [47] and we will make a discussion about these results in the present work.

We study baryons with hidden charm and $I = 1/2, 3/2$, $J = 1/2, 3/2, 5/2$. We take as coupled channels states with $\eta_c, J/\psi$ and an N or a Δ, and states with $\bar{D}$, $\bar{D}^*$ and Λ_c, Σ_c or Σ_c^*. For the different I, J quantum numbers we have the following space states.

(1) $J = 1/2$, $I = 1/2$
$\eta_c N$, $J/\psi N$, $\bar{D}\Lambda_c$, $\bar{D}\Sigma_c$, $\bar{D}^*\Lambda_c$, $\bar{D}^*\Sigma_c$, $\bar{D}^*\Sigma_c^*$.
(2) $J = 1/2$, $I = 3/2$
$J/\psi\Delta$, $\bar{D}\Sigma_c$, $\bar{D}^*\Sigma_c$, $\bar{D}^*\Sigma_c^*$.
(3) $J = 3/2$, $I = 1/2$
$J/\psi N$, $\bar{D}^*\Lambda_c$, $\bar{D}^*\Sigma_c$, $\bar{D}\Sigma_c^*$, $\bar{D}^*\Sigma_c^*$.
(4) $J = 3/2$, $I = 3/2$
$\eta_c\Delta$, $J/\psi\Delta$, $\bar{D}^*\Sigma_c$, $\bar{D}\Sigma_c^*$, $\bar{D}^*\Sigma_c^*$.
(5) $J = 5/2$, $I = 1/2$
$\bar{D}^*\Sigma_c^*$.
(6) $J = 5/2$, $I = 3/2$
$J/\psi\Delta$, $\bar{D}^*\Sigma_c^*$.

Attending to the spin quantum number, we thus have 17 orthogonal states in the physical basis. Next we will introduce a different basis, which we will call the HQSS basis, for which it is straightforward to implement the LO HQSS constraints. In the HQSS basis we will classify the states in terms of the quantum numbers: J, total spin of the meson-baryon system; $\mathcal{L}$, total spin of the light quark system; $S_{c\bar{c}}$, total spin of the $c\bar{c}$ subsystem; ℓ_M, total spin of the light quarks in the meson and ℓ_B, total spin of the light quarks in the baryon. Note that we assume that all orbital angular momenta are zero since we are dealing with ground-state baryons.

Thus, the 17 orthogonal states in the HQSS basis are given by

(i) $|S_{c\bar{c}} = 0, \mathcal{L} = \frac{1}{2}; J = \frac{1}{2}\rangle_{(\ell_M=0,\ell_B=\frac{1}{2})}$,
$|S_{c\bar{c}} = 0, \mathcal{L} = \frac{1}{2}; J = \frac{1}{2}\rangle_{(\ell_M=1/2,\ell_B=0)}$,
$|S_{c\bar{c}} = 0, \mathcal{L} = \frac{1}{2}; J = \frac{1}{2}\rangle_{(\ell_M=1/2,\ell_B=1)}$,
(ii) $|S_{c\bar{c}} = 1, \mathcal{L} = \frac{1}{2}; J = \frac{1}{2}\rangle_{(\ell_M=0,\ell_B=\frac{1}{2})}$,
$|S_{c\bar{c}} = 1, \mathcal{L} = \frac{1}{2}; J = \frac{1}{2}\rangle_{(\ell_M=1/2,\ell_B=0)}$,
$|S_{c\bar{c}} = 1, \mathcal{L} = \frac{1}{2}; J = \frac{1}{2}\rangle_{(\ell_M=1/2,\ell_B=1)}$,
(iii) $|S_{c\bar{c}} = 1, \mathcal{L} = \frac{1}{2}; J = \frac{3}{2}\rangle_{(\ell_M=0,\ell_B=\frac{1}{2})}$,
$|S_{c\bar{c}} = 1, \mathcal{L} = \frac{1}{2}; J = \frac{3}{2}\rangle_{(\ell_M=1/2,\ell_B=0)}$,
$|S_{c\bar{c}} = 1, \mathcal{L} = \frac{1}{2}; J = \frac{3}{2}\rangle_{(\ell_M=1/2,\ell_B=1)}$,
(iv) $|S_{c\bar{c}} = 0, \mathcal{L} = \frac{3}{2}; J = \frac{3}{2}\rangle_{(\ell_M=0,\ell_B=\frac{3}{2})}$,
$|S_{c\bar{c}} = 0, \mathcal{L} = \frac{3}{2}; J = \frac{3}{2}\rangle_{(\ell_M=1/2,\ell_B=1)}$,
(v) $|S_{c\bar{c}} = 1, \mathcal{L} = \frac{3}{2}; J = \frac{1}{2}\rangle_{(\ell_M=0,\ell_B=\frac{3}{2})}$,
$|S_{c\bar{c}} = 1, \mathcal{L} = \frac{3}{2}; J = \frac{1}{2}\rangle_{(\ell_M=1/2,\ell_B=1)}$,
(vi) $|S_{c\bar{c}} = 1, \mathcal{L} = \frac{3}{2}; J = \frac{3}{2}\rangle_{(\ell_M=0,\ell_B=\frac{3}{2})}$,
$|S_{c\bar{c}} = 1, \mathcal{L} = \frac{3}{2}; J = \frac{3}{2}\rangle_{(\ell_M=1/2,\ell_B=1)}$,
(vii) $|S_{c\bar{c}} = 1, \mathcal{L} = \frac{3}{2}; J = \frac{5}{2}\rangle_{(\ell_M=0,\ell_B=\frac{3}{2})}$,
$|S_{c\bar{c}} = 1, \mathcal{L} = \frac{3}{2}; J = \frac{5}{2}\rangle_{(\ell_M=1/2,\ell_B=1)}$.

The approximate HQSS of QCD leads [neglecting $\mathcal{O}(\Lambda_{\rm QCD}/m_Q)$ corrections] to important simplifications when the HQSS basis is used:

$$_{(\ell'_M,\ell'_B)}\langle S'_{c\bar{c}},\,\mathcal{L}';J',\,\alpha'|H^{\rm QCD}|S_{c\bar{c}},\,\mathcal{L};J,\,\alpha\rangle_{(\ell_M,\ell_B)}=\delta_{\alpha\alpha'}\delta_{JJ'}\delta_{S'_{c\bar{c}}S_{c\bar{c}}}\delta_{\mathcal{L}\mathcal{L}'}\langle\ell'_M\ell'_B\mathcal{L};\alpha||H^{\rm QCD}||\ell_M\ell_B\mathcal{L};\alpha\rangle, \tag{1}$$

where α stands for other quantum numbers (isospin and hypercharge), which are conserved by QCD. Note that the reduced matrix elements do not depend on $S_{c\bar{c}}$ because QCD dynamics is invariant under separate spin rotations of the charm quark and antiquark. Thus, one can transform a $c\bar{c}$ spin singlet state into a spin triplet state by means of a rotation that commutes with $H^{\rm QCD}$, i.e., without cost of energy. Thus, in a given α sector, we have a total of nine unknown low energy constants (LEC's):

(i) Three LEC's associated with $\mathcal{L}=3/2$,

$$\lambda_1^\alpha=\left\langle\ell'_M=0,\,\ell'_B=\frac{3}{2},\,\mathcal{L}=3/2;\alpha\|H^{\rm QCD}\|\ell_M=0,\,\ell_B=\frac{3}{2},\,\mathcal{L}=3/2;\alpha\right\rangle, \tag{2}$$

$$\lambda_2^\alpha=\langle\ell'_M=1/2,\,\ell'_B=1,\,\mathcal{L}=3/2;\alpha\|H^{\rm QCD}\|\ell_M=1/2,\,\ell_B=1,\,\mathcal{L}=3/2;\alpha\rangle, \tag{3}$$

$$\lambda_{12}^\alpha=\left\langle\ell'_M=0,\,\ell'_B=\frac{3}{2},\,\mathcal{L}=3/2;\alpha\|H^{\rm QCD}\|\ell_M=1/2,\,\ell_B=1,\,\mathcal{L}=3/2;\alpha\right\rangle. \tag{4}$$

(ii) Six LEC's associated with $\mathcal{L}=1/2$,

$$\mu_1^\alpha=\left\langle\ell'_M=0,\,\ell'_B=\frac{1}{2},\,\mathcal{L}=1/2;\alpha\|H^{\rm QCD}\|\ell_M=0,\,\ell_B=\frac{1}{2},\,\mathcal{L}=1/2;\alpha\right\rangle, \tag{5}$$

$$\mu_2^\alpha=\langle\ell'_M=1/2,\,\ell'_B=0,\,\mathcal{L}=1/2;\alpha\|H^{\rm QCD}\|\ell_M=1/2,\,\ell_B=0,\,\mathcal{L}=1/2;\alpha\rangle, \tag{6}$$

$$\mu_3^\alpha=\langle\ell'_M=1/2,\,\ell'_B=1,\,\mathcal{L}=1/2;\alpha\|H^{\rm QCD}\|\ell_M=1/2,\,\ell_B=1,\,\mathcal{L}=1/2;\alpha\rangle, \tag{7}$$

$$\mu_{12}^\alpha=\left\langle\ell'_M=0,\,\ell'_B=\frac{1}{2},\,\mathcal{L}=1/2;\alpha\|H^{\rm QCD}\|\ell_M=1/2,\,\ell_B=0,\,\mathcal{L}=1/2;\alpha\right\rangle, \tag{8}$$

$$\mu_{13}^\alpha=\left\langle\ell'_M=0,\,\ell'_B=\frac{1}{2},\,\mathcal{L}=1/2;\alpha\|H^{\rm QCD}\|\ell_M=1/2,\,\ell_B=1,\,\mathcal{L}=1/2;\alpha\right\rangle, \tag{9}$$

$$\mu_{23}^\alpha=\langle\ell'_M=1/2,\,\ell'_B=0,\,\mathcal{L}=1/2;\alpha\|H^{\rm QCD}\|\ell_M=1/2,\,\ell_B=1,\,\mathcal{L}=1/2;\alpha\rangle. \tag{10}$$

This means that in the HQSS basis, the $H^{\rm QCD}$ is a block-diagonal matrix, i.e., up to $\mathcal{O}(\Lambda_{\rm QCD}/m_Q)$ corrections, $H^{\rm QCD}=\mathrm{Diag}(\mu^\alpha,\,\mu^\alpha,\,\mu^\alpha,\,\lambda^\alpha,\,\lambda^\alpha,\,\lambda^\alpha,\,\lambda^\alpha)$, where μ^α and λ^α are symmetric matrices of dimensions 3 and 2, respectively.

To exploit Eq. (1), one should express hidden charm uncoupled meson-baryon states in terms of the HQSS basis. For those states composed of hidden charm mesons ($\ell_M=0$) the relations are trivial,

$$\left|\eta_cN;J=\frac{1}{2}\right\rangle=\left|S_{c\bar{c}}=0,\,\mathcal{L}=\frac{1}{2};J=\frac{1}{2}\right\rangle_{(\ell_M=0,\ell_B=\frac{1}{2})}, \tag{11}$$

$$\left|\eta_c\Delta;J=\frac{3}{2}\right\rangle=\left|S_{c\bar{c}}=0,\,\mathcal{L}=\frac{3}{2};J=\frac{3}{2}\right\rangle_{(\ell_M=0,\ell_B=\frac{3}{2})}, \tag{12}$$

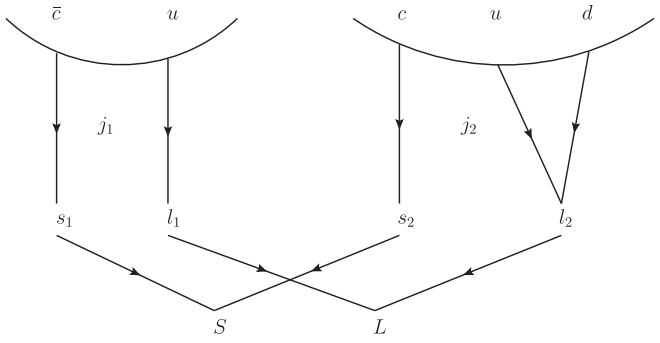

FIG. 1. Diagrams for the 9-j coefficients evaluation.

$$\left|J_\Psi N; J=\frac{1}{2}\right\rangle = \left|S_{c\bar{c}}=1, \mathcal{L}=\frac{1}{2}; J=\frac{1}{2}\right\rangle_{(\ell_M=0,\ell_B=\frac{1}{2})}, \tag{13}$$

$$\left|J_\Psi N; J=\frac{3}{2}\right\rangle = \left|S_{c\bar{c}}=1, \mathcal{L}=\frac{1}{2}; J=\frac{3}{2}\right\rangle_{(\ell_M=0,\ell_B=\frac{1}{2})}, \tag{14}$$

$$\left|J_\Psi \Delta; J=\frac{1}{2}\right\rangle = \left|S_{c\bar{c}}=1, \mathcal{L}=\frac{3}{2}; J=\frac{1}{2}\right\rangle_{(\ell_M=0,\ell_B=\frac{3}{2})}, \tag{15}$$

$$\left|J_\Psi \Delta; J=\frac{3}{2}\right\rangle = \left|S_{c\bar{c}}=1, \mathcal{L}=\frac{3}{2}; J=\frac{3}{2}\right\rangle_{(\ell_M=0,\ell_B=\frac{3}{2})}, \tag{16}$$

$$\left|J_\Psi \Delta; J=\frac{5}{2}\right\rangle = \left|S_{c\bar{c}}=1, \mathcal{L}=\frac{3}{2}; J=\frac{5}{2}\right\rangle_{(\ell_M=0,\ell_B=\frac{3}{2})}, \tag{17}$$

while for the other states, one needs to use 9-j symbols.

The 9-j symbols are used to relate two bases where the angular momentums are coupled in a different way. Taking two particles with $\vec{l}_1$, $\vec{s}_1$ and $\vec{l}_2$, $\vec{s}_2$, we can combine them with $\vec{j}_1$, $\vec{j}_2$ and finally $\vec{j}_1$, $\vec{j}_2$ to obtain a total $\vec{J}$. Alternatively, we can couple $\vec{l}_1$, $\vec{l}_2$ to $\vec{L}$, $\vec{s}_1$, $\vec{s}_2$ to $\vec{S}$, and then $\vec{L}$, $\vec{S}$ to a total $\vec{J}$. These two bases are related as [55]

$$|l_1 s_1 j_1; l_2 s_2 j_2; JM\rangle = \sum_{S,L}[(2S+1)(2L+1)(2j_1+1)(2j_2+1)]^{1/2} \begin{Bmatrix} l_1 & l_2 & L \\ s_1 & s_2 & S \\ j_1 & j_2 & J \end{Bmatrix} |l_1 l_2 L; s_1 s_2 S; JM\rangle, \tag{18}$$

where the symbol $\{\ \}$ stands for the 9-j coefficients.

As an example, take a meson-baryon (M-B) state of the type $\bar{D}^{(*)}B_c$ and look at the recombination scheme in Fig. 1. Thus, in this case we have the correspondence

$$\begin{array}{lccccccccc} \text{generic: } & l_1 & & l_2 & s_1 & s_2 & j_1 & j_2 & L & S & J \\ \text{HQSS: } & \ell_M\left(\frac{1}{2}\right) & & \ell_B & \frac{1}{2} & \frac{1}{2} & J_M(0,1) & J_B\left(\frac{1}{2},\frac{3}{2}\right) & \mathcal{L} & S_{c\bar{c}} & J\left(\frac{1}{2},\frac{3}{2},\frac{5}{2}\right). \end{array}$$

with J_M and J_B the total spin of the meson and baryon, respectively. Then one easily finds

(i) $J = 1/2$,

$$|\bar{D}\Lambda_c\rangle = \frac{1}{2}\left|S_{c\bar{c}}=0, \mathcal{L}=\frac{1}{2}; J=\frac{1}{2}\right\rangle_{(\ell_M=1/2,\ell_B=0)} + \frac{\sqrt{3}}{2}\left|S_{c\bar{c}}=1, \mathcal{L}=\frac{1}{2}; J=\frac{1}{2}\right\rangle_{(\ell_M=1/2,\ell_B=0)}, \tag{19}$$

$$\begin{aligned} |\bar{D}\Sigma_c\rangle = {} & \frac{1}{2}\left|S_{c\bar{c}}=0, \mathcal{L}=\frac{1}{2}; J=\frac{1}{2}\right\rangle_{(\ell_M=1/2,\ell_B=1)} - \frac{1}{2\sqrt{3}}\left|S_{c\bar{c}}=1, \mathcal{L}=\frac{1}{2}; J=\frac{1}{2}\right\rangle_{(\ell_M=1/2,\ell_B=1)} \\ & + \sqrt{\frac{2}{3}}\left|S_{c\bar{c}}=1, \mathcal{L}=\frac{3}{2}; J=\frac{1}{2}\right\rangle_{(\ell_M=1/2,\ell_B=1)}, \end{aligned} \tag{20}$$

$$|\bar{D}^*\Lambda_c\rangle = \frac{\sqrt{3}}{2}\left|S_{c\bar{c}}=0, \mathcal{L}=\frac{1}{2}; J=\frac{1}{2}\right\rangle_{(\ell_M=1/2,\ell_B=0)} - \frac{1}{2}\left|S_{c\bar{c}}=1, \mathcal{L}=\frac{1}{2}; J=\frac{1}{2}\right\rangle_{(\ell_M=1/2,\ell_B=0)}, \tag{21}$$

$$|\bar{D}^*\Sigma_c\rangle = -\frac{1}{\sqrt{12}}\left|S_{c\bar{c}}=0,\mathcal{L}=\frac{1}{2};J=\frac{1}{2}\right\rangle_{(\ell_M=1/2,\ell_B=1)}+\frac{5}{6}\left|S_{c\bar{c}}=1,\mathcal{L}=\frac{1}{2};J=\frac{1}{2}\right\rangle_{(\ell_M=1/2,\ell_B=1)}$$
$$+\frac{\sqrt{2}}{3}\left|S_{c\bar{c}}=1,\mathcal{L}=\frac{3}{2};J=\frac{1}{2}\right\rangle_{(\ell_M=1/2,\ell_B=1)}, \tag{22}$$

$$|\bar{D}^*\Sigma_c^*\rangle = \frac{2}{\sqrt{6}}\left|S_{c\bar{c}}=0,\mathcal{L}=\frac{1}{2};J=\frac{1}{2}\right\rangle_{(\ell_M=1/2,\ell_B=1)}+\frac{\sqrt{2}}{3}\left|S_{c\bar{c}}=1,\mathcal{L}=\frac{1}{2};J=\frac{1}{2}\right\rangle_{(\ell_M=1/2,\ell_B=1)}$$
$$-\frac{1}{3}\left|S_{c\bar{c}}=1,\mathcal{L}=\frac{3}{2};J=\frac{1}{2}\right\rangle_{(\ell_M=1/2,\ell_B=1)}. \tag{23}$$

(ii) $J = 3/2$,

$$|\bar{D}^*\Lambda_c\rangle = \left|S_{c\bar{c}}=1,\mathcal{L}=\frac{1}{2};J=\frac{3}{2}\right\rangle_{(\ell_M=1/2,\ell_B=0)}, \tag{24}$$

$$|\bar{D}^*\Sigma_c\rangle = -\frac{1}{\sqrt{3}}\left|S_{c\bar{c}}=0,\mathcal{L}=\frac{3}{2};J=\frac{3}{2}\right\rangle_{(\ell_M=1/2,\ell_B=1)}+\frac{1}{3}\left|S_{c\bar{c}}=1,\mathcal{L}=\frac{1}{2};J=\frac{3}{2}\right\rangle_{(\ell_M=1/2,\ell_B=1)}$$
$$+\frac{\sqrt{5}}{3}\left|S_{c\bar{c}}=1,\mathcal{L}=\frac{3}{2};J=\frac{3}{2}\right\rangle_{(\ell_M=1/2,\ell_B=1)}, \tag{25}$$

$$|\bar{D}\Sigma_c^*\rangle = \frac{1}{2}\left|S_{c\bar{c}}=0,\mathcal{L}=\frac{3}{2};J=\frac{3}{2}\right\rangle_{(\ell_M=1/2,\ell_B=1)}-\frac{1}{\sqrt{3}}\left|S_{c\bar{c}}=1,\mathcal{L}=\frac{1}{2};J=\frac{3}{2}\right\rangle_{(\ell_M=1/2,\ell_B=1)}$$
$$+\sqrt{\frac{5}{12}}\left|S_{c\bar{c}}=1,\mathcal{L}=\frac{3}{2};J=\frac{3}{2}\right\rangle_{(\ell_M=1/2,\ell_B=1)}, \tag{26}$$

$$|\bar{D}^*\Sigma_c^*\rangle = \sqrt{\frac{5}{12}}\left|S_{c\bar{c}}=0,\mathcal{L}=\frac{3}{2};J=\frac{3}{2}\right\rangle_{(\ell_M=1/2,\ell_B=1)}+\frac{\sqrt{5}}{3}\left|S_{c\bar{c}}=1,\mathcal{L}=\frac{1}{2};J=\frac{3}{2}\right\rangle_{(\ell_M=1/2,\ell_B=1)}$$
$$+\frac{1}{6}\left|S_{c\bar{c}}=1,\mathcal{L}=\frac{3}{2};J=\frac{3}{2}\right\rangle_{(\ell_M=1/2,\ell_B=1)}. \tag{27}$$

(iii) $J = 5/2$,

$$|\bar{D}^*\Sigma_c^*\rangle = \left|S_{c\bar{c}}=1,\mathcal{L}=\frac{3}{2};J=\frac{5}{2}\right\rangle_{(\ell_M=1/2,\ell_B=1)}. \tag{28}$$

Ignoring hidden strange channels, we find the following interactions for each sector (these are the most general interactions compatible with HQSS):

(i) $J = 1/2$, $I = 1/2$,

$$\begin{array}{c} \begin{matrix} \eta_c N & J_\Psi N & \bar{D}\Lambda_c & \bar{D}\Sigma_c & \bar{D}^*\Lambda_c & \bar{D}^*\Sigma_c & \bar{D}^*\Sigma_c^* \end{matrix} \\ \begin{pmatrix} \mu_1 & 0 & \frac{\mu_{12}}{2} & \frac{\mu_{13}}{2} & \frac{\sqrt{3}\mu_{12}}{2} & -\frac{\mu_{13}}{2\sqrt{3}} & \sqrt{\frac{2}{3}}\mu_{13} \\ 0 & \mu_1 & \frac{\sqrt{3}\mu_{12}}{2} & -\frac{\mu_{13}}{2\sqrt{3}} & -\frac{\mu_{12}}{2} & \frac{5\mu_{13}}{6} & \frac{\sqrt{2}\mu_{13}}{3} \\ \frac{\mu_{12}}{2} & \frac{\sqrt{3}\mu_{12}}{2} & \mu_2 & 0 & 0 & \frac{\mu_{23}}{\sqrt{3}} & \sqrt{\frac{2}{3}}\mu_{23} \\ \frac{\mu_{13}}{2} & -\frac{\mu_{13}}{2\sqrt{3}} & 0 & \frac{1}{3}(2\lambda_2+\mu_3) & \frac{\mu_{23}}{\sqrt{3}} & \frac{2(\lambda_2-\mu_3)}{3\sqrt{3}} & \frac{1}{3}\sqrt{\frac{2}{3}}(\mu_3-\lambda_2) \\ \frac{\sqrt{3}\mu_{12}}{2} & -\frac{\mu_{12}}{2} & 0 & \frac{\mu_{23}}{\sqrt{3}} & \mu_2 & -\frac{2\mu_{23}}{3} & \frac{\sqrt{2}\mu_{23}}{3} \\ -\frac{\mu_{13}}{2\sqrt{3}} & \frac{5\mu_{13}}{6} & \frac{\mu_{23}}{\sqrt{3}} & \frac{2(\lambda_2-\mu_3)}{3\sqrt{3}} & -\frac{2\mu_{23}}{3} & \frac{1}{9}(2\lambda_2+7\mu_3) & \frac{1}{9}\sqrt{2}(\mu_3-\lambda_2) \\ \sqrt{\frac{2}{3}}\mu_{13} & \frac{\sqrt{2}\mu_{13}}{3} & \sqrt{\frac{2}{3}}\mu_{23} & \frac{1}{3}\sqrt{\frac{2}{3}}(\mu_3-\lambda_2) & \frac{\sqrt{2}\mu_{23}}{3} & \frac{1}{9}\sqrt{2}(\mu_3-\lambda_2) & \frac{1}{9}(\lambda_2+8\mu_3) \end{pmatrix}_{I=1/2} \end{array}. \tag{29}$$

(ii) $J = 1/2$, $I = 3/2$,

$$\begin{array}{c} \begin{matrix} J_\Psi\Delta & \bar{D}\Sigma_c & \bar{D}^*\Sigma_c & \bar{D}^*\Sigma_c^* \end{matrix} \\ \begin{pmatrix} \lambda_1 & \sqrt{\frac{2}{3}}\lambda_{12} & \frac{\sqrt{2}\lambda_{12}}{3} & -\frac{\lambda_{12}}{3} \\ \sqrt{\frac{2}{3}}\lambda_{12} & \frac{1}{3}(2\lambda_2+\mu_3) & \frac{2(\lambda_2-\mu_3)}{3\sqrt{3}} & \frac{1}{3}\sqrt{\frac{2}{3}}(\mu_3-\lambda_2) \\ \frac{\sqrt{2}\lambda_{12}}{3} & \frac{2(\lambda_2-\mu_3)}{3\sqrt{3}} & \frac{1}{9}(2\lambda_2+7\mu_3) & \frac{1}{9}\sqrt{2}(\mu_3-\lambda_2) \\ -\frac{\lambda_{12}}{3} & \frac{1}{3}\sqrt{\frac{2}{3}}(\mu_3-\lambda_2) & \frac{1}{9}\sqrt{2}(\mu_3-\lambda_2) & \frac{1}{9}(\lambda_2+8\mu_3) \end{pmatrix}_{I=3/2} \end{array}. \tag{30}$$

(iii) $J = 3/2$, $I = 1/2$,

$$\begin{array}{c} \begin{matrix} J_\Psi N & \bar{D}^*\Lambda_c & \bar{D}^*\Sigma_c & \bar{D}\Sigma_c^* & \bar{D}^*\Sigma_c^* \end{matrix} \\ \begin{pmatrix} \mu_1 & \mu_{12} & \frac{\mu_{13}}{3} & -\frac{\mu_{13}}{\sqrt{3}} & \frac{\sqrt{5}\mu_{13}}{3} \\ \mu_{12} & \mu_2 & \frac{\mu_{23}}{3} & -\frac{\mu_{23}}{\sqrt{3}} & \frac{\sqrt{5}\mu_{23}}{3} \\ \frac{\mu_{13}}{3} & \frac{\mu_{23}}{3} & \frac{1}{9}(8\lambda_2+\mu_3) & \frac{\lambda_2-\mu_3}{3\sqrt{3}} & \frac{1}{9}\sqrt{5}(\mu_3-\lambda_2) \\ -\frac{\mu_{13}}{\sqrt{3}} & -\frac{\mu_{23}}{\sqrt{3}} & \frac{\lambda_2-\mu_3}{3\sqrt{3}} & \frac{1}{3}(2\lambda_2+\mu_3) & \frac{1}{3}\sqrt{\frac{5}{3}}(\lambda_2-\mu_3) \\ \frac{\sqrt{5}\mu_{13}}{3} & \frac{\sqrt{5}\mu_{23}}{3} & \frac{1}{9}\sqrt{5}(\mu_3-\lambda_2) & \frac{1}{3}\sqrt{\frac{5}{3}}(\lambda_2-\mu_3) & \frac{1}{9}(4\lambda_2+5\mu_3) \end{pmatrix}_{I=1/2} \end{array}. \tag{31}$$

(iv) $J = 3/2$, $I = 3/2$,

$$\begin{array}{c} \begin{matrix} \eta_c\Delta & J_\Psi\Delta & \bar{D}^*\Sigma_c & \bar{D}\Sigma_c^* & \bar{D}^*\Sigma_c^* \end{matrix} \\ \begin{pmatrix} \lambda_1 & 0 & -\frac{\lambda_{12}}{\sqrt{3}} & \frac{\lambda_{12}}{2} & \frac{1}{2}\sqrt{\frac{5}{3}}\lambda_{12} \\ 0 & \lambda_1 & \frac{\sqrt{5}\lambda_{12}}{3} & \frac{1}{2}\sqrt{\frac{5}{3}}\lambda_{12} & \frac{\lambda_{12}}{6} \\ -\frac{\lambda_{12}}{\sqrt{3}} & \frac{\sqrt{5}\lambda_{12}}{3} & \frac{1}{9}(8\lambda_2+\mu_3) & \frac{\lambda_2-\mu_3}{3\sqrt{3}} & \frac{1}{9}\sqrt{5}(\mu_3-\lambda_2) \\ \frac{\lambda_{12}}{2} & \frac{1}{2}\sqrt{\frac{5}{3}}\lambda_{12} & \frac{\lambda_2-\mu_3}{3\sqrt{3}} & \frac{1}{3}(2\lambda_2+\mu_3) & \frac{1}{3}\sqrt{\frac{5}{3}}(\lambda_2-\mu_3) \\ \frac{1}{2}\sqrt{\frac{5}{3}}\lambda_{12} & \frac{\lambda_{12}}{6} & \frac{1}{9}\sqrt{5}(\mu_3-\lambda_2) & \frac{1}{3}\sqrt{\frac{5}{3}}(\lambda_2-\mu_3) & \frac{1}{9}(4\lambda_2+5\mu_3) \end{pmatrix}_{I=3/2} \end{array}. \tag{32}$$

(v) $J = 5/2$, $I = 1/2$,

$$\begin{matrix} \bar{D}^*\Sigma_c^* \\ (\ \lambda_2\ )_{I=1/2} \end{matrix}. \tag{33}$$

(vi) $J = 5/2$, $I = 3/2$,

$$\begin{matrix} J_\Psi\Delta & \bar{D}^*\Sigma_c^* \\ \begin{pmatrix} \lambda_1 & \lambda_{12} \\ \lambda_{12} & \lambda_2 \end{pmatrix}_{I=3/2} \end{matrix}. \tag{34}$$

We should stress, once more, that μ and λ depend on isospin, and thus those LEC's corresponding to $I = 1/2$ are not the same as those corresponding to $I = 3/2$. However, they can be related using SU(3) flavor symmetry.

There is a total of seven ($6\mu's$ and λ_2) independent LEC's for $I = 1/2$, while for $I = 3/2$, we have four ($3\lambda's$ and μ_3) LEC's. Thus, when one neglects open and hidden strange channels, we have a total of 11 LEC's. The extension of the WT model, using SU(8) spin-flavor symmetry [47], provides predictions for all these LEC's. Namely,

$$\begin{aligned} &I = 1/2 \to \mu_1 = 0, \quad \mu_2 = \mu_3 = 1, \\ &\mu_{12} = -\mu_{13} = \sqrt{6}, \quad \mu_{23} = -3, \quad \lambda_2 = -2; \end{aligned} \tag{35}$$

$$\begin{aligned} &I = 3/2 \to \mu_3 = -2, \qquad \lambda_1 = 0, \\ &\lambda_{12} = 2\sqrt{3}, \qquad \lambda_2 = 4, \end{aligned} \tag{36}$$

up to an overall $\frac{1}{4f^2}(k^0 + k'^0)$ factor, with k^0 and k'^0 the center-of-mass energies of the incoming and outgoing mesons. The extension of the local hidden gauge approach to the charm sector provides different values, as we discuss below.

Note that in [47] (Sec. II.F) the 12 most general operators allowed by SU(3) $\times$ HQSS in the hidden charm baryon-meson sector were already given. Moreover, the reduction of these Lagrangians when no strangeness is involved was also discussed. In this latter case, there are 11 independent couplings, which determine the 11 LEC's ($\mu's$ and $\lambda's$) introduced in Eqs. (29)–(34).

III. BRIEF DESCRIPTION OF THE LOCAL HIDDEN GAUGE FORMALISM

We summarize the formalism of the hidden gauge interaction for vector mesons, which we take from [3,4] (see also useful Feynman rules in [56]) extended to SU(4). The Lagrangian accounting for the interaction of vector mesons amongst themselves is given by

$$\mathcal{L}_{III} = -\frac{1}{4}\langle V_{\mu\nu}V^{\mu\nu}\rangle, \tag{37}$$

where the $\langle\ \rangle$ symbol represents the trace in the SU(4) space and $V_{\mu\nu}$ is given by

$$V_{\mu\nu} = \partial_\mu V_\nu - \partial_\nu V_\mu - ig[V_\mu, V_\nu], \tag{38}$$

with the coupling of the theory given by $g = \frac{M_V}{2f}$, where $f = 93$ MeV is the pion decay constant. The magnitude V_μ is the SU(4) matrix of the vectors of the meson 15-plet + singlet, given by [57]

$$V_\mu = \begin{pmatrix} \frac{\rho^0}{\sqrt{2}} + \frac{\omega}{\sqrt{2}} & \rho^+ & K^{*+} & \bar{D}^{*0} \\ \rho^- & -\frac{\rho^0}{\sqrt{2}} + \frac{\omega}{\sqrt{2}} & K^{*0} & D^{*-} \\ K^{*-} & \bar{K}^{*0} & \phi & D_s^{*-} \\ D^{*0} & D^{*+} & D_s^{*+} & J/\psi \end{pmatrix}_\mu. \tag{39}$$

The interaction of $\mathcal{L}_{III}$ provides a contact term that comes from $[V_\mu, V_\nu][V_\mu, V_\nu]$,

$$\mathcal{L}_{III}^{(c)} = \frac{g^2}{2}\langle V_\mu V_\nu V^\mu V^\nu - V_\nu V_\mu V^\mu V^\nu\rangle, \tag{40}$$

as well as a three vector vertex from

$$\begin{aligned} \mathcal{L}_{III}^{(3V)} &= ig\langle(\partial_\mu V_\nu - \partial_\nu V_\mu)V^\mu V^\nu\rangle \\ &= ig\langle(V^\mu\partial_\nu V_\mu - \partial_\nu V_\mu V^\mu)V^\nu\rangle. \end{aligned} \tag{41}$$

It is worth recalling the analogy with the coupling of vectors to pseudoscalars given in the same formalism by

$$\mathcal{L}_{VPP} = -ig\langle[P, \partial_\mu P]V^\mu\rangle, \tag{42}$$

where P is the SU(4) matrix of the pseudoscalar fields,

$$P = \begin{pmatrix} \frac{\pi^0}{\sqrt{2}} + \frac{\eta_8}{\sqrt{6}} + \frac{\tilde{\eta}_c}{\sqrt{12}} + \frac{\tilde{\eta}_c'}{\sqrt{4}} & \pi^+ & K^+ & \bar{D}^0 \\ \pi^- & -\frac{\pi^0}{\sqrt{2}} + \frac{\eta_8}{\sqrt{6}} + \frac{\tilde{\eta}_c}{\sqrt{12}} + \frac{\tilde{\eta}_c'}{\sqrt{4}} & K^0 & D^- \\ K^- & \bar{K}^0 & \frac{-2\eta_8}{\sqrt{6}} + \frac{\tilde{\eta}_c}{\sqrt{12}} + \frac{\tilde{\eta}_c'}{\sqrt{4}} & D_s^- \\ D^0 & D^+ & D_s^+ & -\frac{3\tilde{\eta}_c}{\sqrt{12}} + \frac{\tilde{\eta}_c'}{\sqrt{4}} \end{pmatrix}. \tag{43}$$

$\tilde{\eta}_c$ stands for the SU(3) singlet of the 15th SU(4) representation, and $\tilde{\eta}_c'$ denotes the singlet of SU(4) (see quark content in [2]). The physical η_c can be written as [2]

$$\eta_c = \frac{1}{2}(-\sqrt{3}\tilde{\eta}_c + \tilde{\eta}_c'). \quad (44)$$

The philosophy of the local hidden gauge in the meson-baryon sector is that the interaction is driven by the exchange of vector mesons, as depicted in Fig. 2. Equations (41) and (42) provide the upper vertex of these Feyman diagrams. It was shown in [24] that the vertices of Eqs. (41) and (42) give rise to the same expression in the limit of small three-momenta of the vector mesons compared to their mass, a limit which is also taken in our calculations. This makes the work technically easy, and it allows the use of many previous results.

The lower vertex, when the baryons belong to the octet of SU(3), is given in terms of the Lagrangian [58,59]

$$\mathcal{L}_{BBV} = g(\langle \bar{B}\gamma_\mu [V^\mu, B]\rangle + \langle \bar{B}\gamma_\mu B\rangle\langle V^\mu\rangle), \quad (45)$$

where B is now the SU(3) matrix of the baryon octet [60,61]. Similarly, one also has a Lagrangian for the coupling of the vector mesons to the baryons of the decuplet, which can be found in [62].

In the charm sector the lower vertex VBB does not have such a simple representation as in SU(3), and in practice one evaluates the matrix elements using SU(4) symmetry by means of Clebsch-Gordan coefficients and reduced matrix elements. This is done in [1,2] [a discussion on the accuracy of the SU(4) symmetry is given there]. Since the 20 representation for baryon states of $3/2^+$ is not considered there, we must consider these matrix elements here. Once again, one uses SU(4) symmetry for this vertex to evaluate the matrix elements, as done in [1,2]. Alternatively, one can use results of SU(3) symmetry, substituting an s quark by a c quark, or make evaluations using wave functions of the quark model [63], substituting the s quark by a c quark.

The γ^μ matrix of the VBB vertex [see Eq. (45)] gets simplified in the approach, where we neglect the three-momenta versus the mass of the particles (in this case the baryon). Thus, only the γ^0 becomes relevant, which can be taken as unity within the baryon states of positive energy that we consider. Then the transition potential corresponding to the diagram of Fig. 2(b) is given by

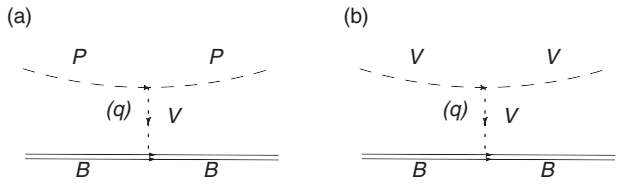

FIG. 2. Diagrams obtained in the effective chiral Lagrangians for the interaction of pseudoscalar (a) or vector (b) mesons with the octet or decuplet of baryons.

$$V_{ij} = -C_{ij}\frac{1}{4f^2}(k^0 + k'^0)\vec{\epsilon}\vec{\epsilon}', \quad (46)$$

where k^0, k'^0 are the energies of the incoming and outgoing vector mesons, and C_{ij} are numerical coefficients evaluated as described above. The expression is the same for the pseudoscalar baryon matrix elements for the same quark content of pseudoscalar and vector mesons, omitting the $\vec{\epsilon}\vec{\epsilon}'$ factor.

The scattering matrix is evaluated by solving the coupled channels Bethe-Salpeter equation in the on-shell factorization approach of [64–66],

$$T = [1 - VG]^{-1}V, \quad (47)$$

with G being the loop function of a meson and a baryon, which we calculate in dimensional regularization using the formula of [65] and similar values for the subtraction constants.

The iteration of diagrams produced by the Bethe-Salpeter equation in the case of the vector mesons keeps the $\vec{\epsilon}\vec{\epsilon}'$ factor in each of the terms. Hence, the factor $\vec{\epsilon}\vec{\epsilon}'$ appearing in the potential V also factorizes in the T matrix for the external vector mesons. A consequence of this is that the interaction is spin independent, and one finds degenerate states having $J^P = 1/2^-$ and $J^P = 3/2^-$.

In the present work, in the spirit of the heavy quark symmetry, we shall include in the coupled channels dynamics the pseudoscalars, vectors, baryons of spin $J = 1/2$, and baryons of $J = 3/2$ using the matrices of Eqs. (29)–(34).

IV. EVALUATION OF THE HQSS LEC'S IN THE LOCAL HIDDEN GAUGE APPROACH

Let us examine first the $I = 1/2$ sector. As an example let us take $\bar{D}\Lambda_c \to \bar{D}\Lambda_c$ and $\bar{D}^*\Lambda_c \to \bar{D}^*\Lambda_c$. These two interactions are equal, as we discussed. This is in agreement with the general HQSS constraints explicited in Eq. (29) for $J = 1/2$ and $I = 1/2$, where both matrix elements are equal to the LEC's μ_2, and it is also consistent with the diagonal $\bar{D}^*\Lambda_c$ entry in Eq. (31) ($J = 3/2$, $I = 1/2$). So we see that the HQSS is respected by the local hidden gauge results. In addition, the interactions of $\bar{D}\Sigma_c \to \bar{D}\Sigma_c$ and $\bar{D}^*\Sigma_c \to \bar{D}^*\Sigma_c$ are also equal. This does not contradict Eqs. (29) and (31); it simply forces

$$\frac{1}{3}(2\lambda_2 + \mu_3) = \frac{1}{9}(2\lambda_2 + 7\mu_3), \quad (48)$$

which has the solution

$$\lambda_2 = \mu_3. \quad (49)$$

As a consequence, the matrix element of $\bar{D}^*\Sigma_c^* \to \bar{D}^*\Sigma_c^*$ is also equal to λ_2. The evaluation of this latter matrix element using SU(4) Clebsch-Gordan coefficients also tells us that this matrix element is the same as the one of $\bar{D}^*\Sigma_c \to \bar{D}^*\Sigma_c$. Once again, we can see that the constraints

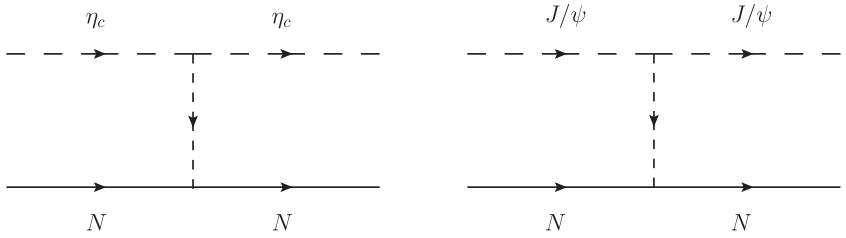

FIG. 3. Diagrams for the $\eta_c N \to \eta_c N$ and $J/\psi N \to J/\psi N$ interactions. No vector-meson exchange is allowed.

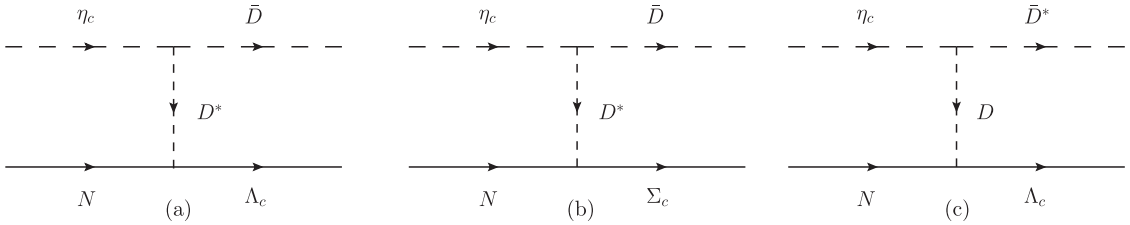

FIG. 4. Diagrams for the $\eta_c N \to \bar{D}\Lambda_c$ (a), $\bar{D}\Sigma_c$ (b), $\bar{D}^*\Lambda_c$ (c) interactions.

of HQSS are fulfilled by the hidden gauge formalism, except that it gives us $\lambda_2 = \mu_3$, which is a different result than the one obtained in the approach of [47] [see Eq. (35)].

Let us look at the coefficient μ_1. It is related to the $\eta_c N \to \eta_c N$ or $J/\psi N \to J/\psi N$ matrix elements. In this case, since η_c or J/ψ have $c\bar{c}$, there is no vector that can be exchanged in Fig. 3, and hence this leads to

$$\mu_1 = 0. \tag{50}$$

This also occurs in the approach of [47], and it is a consequence of the OZI rule that is implemented in both schemes. Let us now look at the μ_{12} parameter. This enters in the $\eta_c N \to \bar{D}\Lambda_c$ transition, which is depicted in Fig. 4(a). Within the hidden gauge model, the diagram forces the exchange of a D^* and is subleading in the m_Q counting [$\mathcal{O}(m_Q^{-2})$]. In the limit of $m_Q \to \infty$ this term would vanish. We, however, keep it and take it from [1,2]. Yet, because it is subleading we shall not expect the LO HQSS restrictions to hold. We also evaluate the diagram of Fig. 4(b), and using again SU(4) symmetry for the $D^* N \Sigma_c$ vertex (see [1,2]) we find that

$$\frac{\mu_{13}}{2} = -\frac{\mu_{12}}{2} \Rightarrow \mu_{13} = -\mu_{12}, \tag{51}$$

which also occurs in [47].

The transition from $\eta_c N \to \bar{D}^*\Lambda_c$ is mediated by the exchange of a D meson; see Fig. 4(c). This term is doubly suppressed because of the D propagator and because of the Yukawa coupling, $\vec{\sigma}\cdot\vec{q}$, in the $DN\Lambda_c$ vertex, where the three-momentum is small compared with m_D. In Eq. (29) we see that this term is proportional to μ_{12}, showing again that the LO HQSS constraint does not hold for these subleading terms in the m_Q counting. In practice, keeping this term, and those for $\eta_c N \to \bar{D}^*\Sigma_c$, $\bar{D}^*\Sigma_c^*$, or ignoring them has no practical repercussions on the final results.

A. Transition from $\bar{D}$ to $\bar{D}^*$

With the dynamics of the local hidden gauge approach, only the pion exchange in the t channel is allowed in this case; see Fig. 5. The $\bar{D}\Lambda_c \to \bar{D}^*\Lambda_c$ transition is zero because the π exchange is zero in the $\pi\Lambda_c\Lambda_c$ vertex. This agrees with the result of the matrix of Eqs. (29), (31), and (33). However the transition $\bar{D}\Lambda_c \to \bar{D}^*\Sigma_c$ is not null and we evaluate it here.

The $\pi\Lambda_c\Sigma_c$ vertex can be obtained by analogy to the $\pi\Lambda\Sigma$ vertex in SU(3) (exchanging the c and s quarks) and using the Lagrangian

$$\mathcal{L} = \frac{1}{2} D\langle \bar{B}\gamma^\mu\gamma_5\{u_\mu, B\}\rangle + \frac{1}{2} F\langle \bar{B}\gamma^\mu\gamma_5[u_\mu, B]\rangle, \tag{52}$$

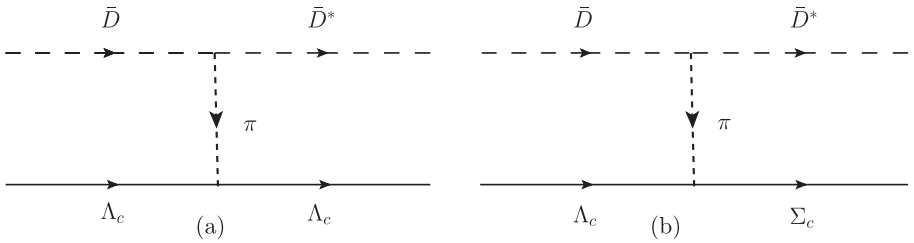

FIG. 5. Diagrams for the pion exchange in the transition of $\bar{D}$, $\bar{D}^*$. Panels (a) and (b) correspond to the $\bar{D}\Lambda_c \to \bar{D}^*\Lambda_c$ and $\bar{D}\Lambda_c \to \bar{D}^*\Sigma_c$ transitions, respectively.

where $u_\mu = iu^\dagger \partial_\mu U u^\dagger$, $u^2 = U = e^{i\sqrt{2}\phi/f}$ with $D = 0.80$, $F = 0.46$ from [67]. The $\bar{D}\bar{D}^*\pi$ vertex is evaluated from Eq. (42). We find, at the end, projecting over an s wave,

$$-it = \frac{1}{\sqrt{6}} \frac{M_V}{2f} \frac{2}{5} \frac{D+F}{2f} \vec{q}^2 \vec{\sigma} \cdot \vec{\epsilon} \frac{i}{q^{02} - \vec{q}^2 - m_\pi^2}, \tag{53}$$

with $\vec{q}$ the momentum transfer.

One can also prove that the matrix element of $\vec{\sigma} \cdot \vec{\epsilon}$ is $\sqrt{3}$ [26]. If we compare the contribution of this diagram with that of the $\bar{D}\Lambda_c \to \bar{D}\Lambda_c$ transition from [1,2], we find a contribution of the order of 7%. If one looks at diagonal matrix elements in the final scattering T matrix, the nondiagonal terms of the transition potentials become squared, and then we can safely neglect this contribution. Thus, we take

$$\mu_{23} = 0. \tag{54}$$

Note that the transitions $\bar{D}\Sigma_c \to \bar{D}^*\Sigma_c$, $\bar{D}^*\Sigma_c^*$ also require the pion exchange and should be taken to be zero. This is consistent with the matrix of Eq. (29) since these matrix elements are proportional to $\lambda_2 - \mu_3$, but we saw before that $\lambda_2 = \mu_3$.

When evaluating the pion exchange mechanism in the $VB \to VB$ transition, one has to consider the equivalent contact term that in the case of $\gamma N \to \pi N$ scattering is known as the Kroll-Ruderman term. Explicit expressions to obtain this term can be found in [26–29], and it is of the same order of magnitude as the pion exchange term, usually with destructive interference. We do not need to evaluate it explicitly here because the important point is that, as in Eq. (53), it is of order $\mathcal{O}(1)$ in the m_Q counting for the field theoretical potential, which implies $\mathcal{O}(m_Q^{-1})$ for the ordinary potential of quantum mechanics, as we shall see in the next section.

With this exercise we have proved that the dynamics of the local hidden gauge approach is fully consistent with the HQSS requirements for the matrix of Eq. (29). The values for the parameters that we obtain from [1,2], together with those determined here, are

$$\begin{aligned} &\mu_2 = \frac{1}{4f^2}(k^0 + k'^0), \qquad \mu_3 = -\frac{1}{4f^2}(k^0 + k'^0), \\ &\mu_{12} = -\sqrt{6}\frac{m_\rho^2}{p_{D^*}^2 - m_{D^*}^2}\frac{1}{4f^2}(k^0 + k'^0), \qquad \mu_1 = 0, \\ &\mu_{23} = 0, \qquad \lambda_2 = \mu_3, \qquad \mu_{13} = -\mu_{12}. \end{aligned} \tag{55}$$

μ_{12} is small, of the order of 15%, but we keep it since this term is the only one that allows the scattering $\eta_c N \to \eta_c N$ ($J/\psi N \to J/\psi N$) through intermediate inelastic states.

The matrix of Eq. (30) for $J = 1/2$ and $I = 3/2$ is equally analyzed. We find

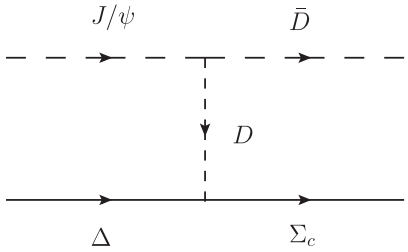

FIG. 6. Diagrams for the $J/\psi\Delta \to \bar{D}\Sigma_c$ interaction.

$$\lambda_1 = 0. \tag{56}$$

Then λ_{12} is also suppressed since it requires again the exchange of a D meson; see Fig. 6. Once again, since the $\bar{D}\Sigma_c \to \bar{D}\Sigma_c$ transition is equivalent to $\bar{D}^*\Sigma_c \to \bar{D}^*\Sigma_c$, this implies that

$$\frac{1}{3}(2\lambda_2 + \mu_3) = \frac{1}{9}(2\lambda_2 + 7\mu_3), \tag{57}$$

from which we conclude again that

$$\lambda_2 = \mu_3. \tag{58}$$

As before, the $\bar{D}\Sigma_c \to \bar{D}^*\Sigma_c$, $\bar{D}\Sigma_c^*$ transitions involve pion exchange, and we find them negligible, which is compatible with the HQSS requirement since $\mu_3 - \lambda_2 = 0$. The values that we obtain with this isospin combination are then

$$\begin{aligned} &\lambda_{12} = 3\sqrt{3}\frac{m_\rho^2}{p_{D^*}^2 - m_{D^*}^2}\frac{1}{4f^2}(k^0 + k'^0), \\ &\mu_3 = 2\frac{1}{4f^2}(k^0 + k'^0), \qquad \lambda_2 = \mu_3, \qquad \lambda_1 = 0. \end{aligned} \tag{59}$$

For Eq. (31) ($J = 3/2, I = 1/2$), since our interaction is spin independent for $PB \to PB$ and of the type $\vec{\epsilon}\vec{\epsilon}'$ for $VB \to VB$, the coefficients are the same as those for Eq. (29) ($J = 1/2, I = 1/2$), given in Eq. (55).

The same can be said for the matrix of Eq. (32) with respect to the one of Eq. (30), as given in Eq. (59).

As for Eq. (33), once again $\bar{D}^*\Sigma_c^* \to \bar{D}^*\Sigma_c^*$ has the same matrix element as $\bar{D}^*\Sigma_c^* \to \bar{D}^*\Sigma_c^*$ of Eq. (29) and, indeed, since $\lambda_2 = \mu_3$, $\frac{1}{9}(\lambda_2 + 8\mu_3) = \lambda_2$, which is given in Eq. (55).

Finally, in Eq. (34) $\lambda_1 = 0$ and λ_2, λ_{12} are the same as those given in Eq. (59) ($I = 3/2$).

V. HEAVY QUARK SPIN SYMMETRY IN THE SU(4) EXTENDED HIDDEN GAUGE APPROACH

The origin of the heavy quark spin symmetry in this case is easy to trace. The $PB \to PB$ transitions have no spin dependence. Also, under the approximation that $\vec{q}/M_D$, $\vec{q}/M_{D^*}$ are negligible (consistent with the heavy quark symmetry), the $VB \to VB$ interaction has trivial $\vec{\epsilon}\vec{\epsilon}'$ dependence and no spin dependence of the baryons, which

also leads to spin independence. Also, up to the trivial $\vec{\epsilon}\vec{\epsilon}'$ factor, the $\bar{D}^*B \to \bar{D}^*B$ interaction is the same as the one for $\bar{D}B \to \bar{D}B$.

Heavy quark symmetry also implies that in leading order the potential is independent of the flavor of the heavy quarks in the limit of $m_Q \to \infty$. This is also accomplished by the dynamics of the local hidden gauge approach. This might be surprising since, as seen in Eq. (46), the potential goes like the sum of the energies of the mesons. This obviously grows from the strange to the charm and then to the bottom sector. However, this is the potential in the field theoretical approach. To have an idea of the strength of the interaction, one has to convert this into the ordinary potential that appears in the Schrödinger equation of quantum mechanics. This is done in [68] [Eq. (68) of that reference].

Because of the normalization of the fields ($\sqrt{\frac{2M_B}{2E_B}}$ for baryons and $\frac{1}{\sqrt{2\omega_M}}$ for mesons) we have

$$V^{FT} = \frac{32\pi^3}{2M_B}\sqrt{s}\mu v^{QM} \quad \text{(meson-baryon)}, \tag{60}$$

where μ is the reduced mass of the system, $M_B m_D/(M_B + m_D)$. Considering that the leading potentials go as $k^0 + k'^0$, we find that

$$v^{QM} \sim \frac{\left(1 + \frac{M_B}{m_D}\right)^2}{\frac{1}{2} + \frac{M_B}{m_D} + \frac{M_B^2}{2m_D^2}} \sim \mathcal{O}(m_Q^0), \tag{61}$$

which goes as $\mathcal{O}(1)$ in powers of m_D, both if M_B is a nucleon and if M_B is one charmed baryon.

Incidentally, in the case of a meson-meson interaction the formula is

$$V^{FT} = 32\pi^3\sqrt{s}\mu v^{QM} \quad \text{(meson-meson)}. \tag{62}$$

Here the interaction in field theory goes as $V^{FT} \sim (k^0 + k'^0)(p^0 + p'^0)$ since both meson lines are linked by a vector meson and we have the $(k^0 + k'^0)$ in each vertex. In this case we also find immediately that $V^{QM} \sim \mathcal{O}(1)$. This means that the extrapolation of the rules of the hidden gauge to SU(4) or even to the bottom sector strictly fulfills the rules of LO HQSS. This would justify the work of [69], where a direct extrapolation of the work [1,2] to the beauty sector is done, or of [48], where a direct extrapolation of the Weinberg-Tomozawa term is taken also in the beauty sector.

VI. RESULTS AND DISCUSSION

We use the Bethe-Salpeter equation in Eq. (47) in coupled channels to evaluate the scattering amplitudes. We need the G function, the loop function of the meson-baryon interaction, for which we take the usual dimensional regularization formula [65]

$$G(s) = i\int \frac{d^4q}{(2\pi)^4}\frac{2M_B}{(P-q)^2 - M_B^2 + i\varepsilon}\frac{1}{q^2 - M_P^2 + i\varepsilon}, \tag{63}$$

$$\begin{aligned} &= \frac{2M_B}{16\pi^2}\left\{a_\mu + \ln\frac{M_B^2}{\mu^2} + \frac{M_P^2 - M_B^2 + s}{2s}\ln\frac{M_P^2}{M_B^2}\right. \\ &+ \frac{q_{cm}}{\sqrt{s}}[\ln(s - (M_B^2 - M_P^2) + 2q_{cm}\sqrt{s}) \\ &+ \ln(s + (M_B^2 - M_P^2) + 2q_{cm}\sqrt{s}) \\ &- \ln(-s - (M_B^2 - M_P^2) + 2q_{cm}\sqrt{s}) \\ &\left. - \ln(-s + (M_B^2 - M_P^2) + 2q_{cm}\sqrt{s})]\right\}, \end{aligned} \tag{64}$$

where q is the four-momentum of the meson, q_{cm} the three-momentum of the particle in the center-of-mass frame, and P the total four-momentum of the meson and the baryon; thus, $s = P^2$. This formula avoids an undesired behavior at large energies when one uses a cutoff method with a small cutoff [70]. As done in [1,2], we take $\mu = 1000$ MeV, $a(\mu) = -2.3$ for the parameters in Eq. (64), which are the only free parameters in our present study. We solve the Bethe-Salpeter equation in Eq. (47) in coupled channels and look for poles in the second Riemann sheet when there are open channels, or in the first Riemann sheet when one has stable bound states (see [2,71] for details).

Let $\sqrt{s_p}$ be the complex energy where a pole appears. Close to a pole the amplitude behaves as

$$T_{ij} = \frac{g_i g_j}{\sqrt{s} - \sqrt{s_p}}, \tag{65}$$

where g_i is the coupling of the resonance to the i channel. As one can see in Eq. (65), $g_i g_j$ is the residue of T_{ij} at the pole. For a diagonal transition we have

$$g_i^2 = \lim_{\sqrt{s}\to\sqrt{s_p}} T_{ii}(\sqrt{s} - \sqrt{s_p}). \tag{66}$$

The determination of the couplings gives us an idea of the structure of the states found since, according to [68,72], the couplings are related to the wave function at the origin for each channel.

Let us begin with the $J = 1/2$, $I = 3/2$ sector. We can see in Eq. (59) that the large potentials are repulsive. So, we should not expect any bound states or resonances. Yet, technically, we find bound states in the first Riemann sheet, as one can see in Fig. 7(a) for different channels. However, inspection of the energies tells us that these are states bound by about 250 MeV, a large number for our intuition, even more when we started from a repulsive potential. The reason for this, which forces us to reject these poles on physical grounds, is that the G function below threshold turns out to be positive for large binding energies [see Fig. 7(b) and discussions in [69]], contradicting what we would have for the G function evaluated with any cutoff, or

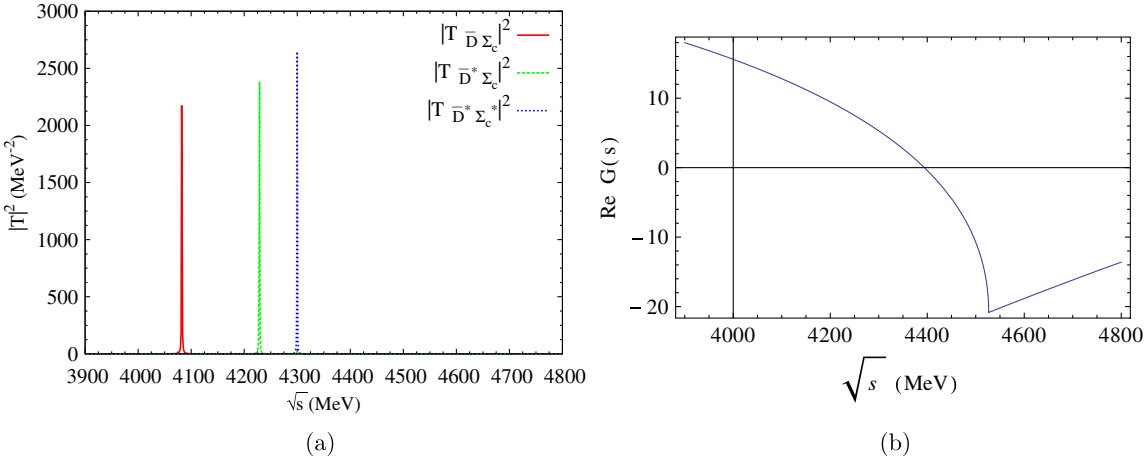

FIG. 7 (color online). The results of the $J = 1/2$, $I = 3/2$ sector. (a): The squared amplitudes of three channels except for the $J/\psi\Delta$ channel. (b): The real parts of the G function in the $\bar{D}^*\Sigma_c^*$ channel.

in quantum mechanics with a given range. These poles are then discarded and, thus, we do not find bound states or resonances in $I = 3/2$ in our approach.

The WT extended model of Ref. [47] predicts $\mu_3 = -2$, which leads to some attractive interactions in the space generated by $\bar{D}^*\Sigma_c$, $\bar{D}\Sigma_c^*$ and $\bar{D}^*\Sigma_c^*$. These give rise to three odd-parity Δ-like resonances (two with spin $1/2$ and one with spin $3/2$) with masses around 4 GeV. In addition, two other states show up as cusps very close to the $\Delta J/\psi$ threshold, and their real existence would be unclear.

Our results for the $J = 1/2, I = 1/2$ sector are shown in Fig. 8. From the squared amplitudes of $|T|^2$, we find three clear peaks with nonzero width around the energy range 4200–4500 MeV, which are not far below the thresholds of $\bar{D}\Sigma_c$, $\bar{D}^*\Sigma_c$, $\bar{D}^*\Sigma_c^*$, respectively. The relatively small width of about 40 MeV of these states allows us to distinguish them clearly. We have checked that in the energy ranges where these peaks appear, the real parts of the loop function G, Eq. (64), are negative in these channels. Thus, these peaks are acceptable as physical ones. Then, because of the

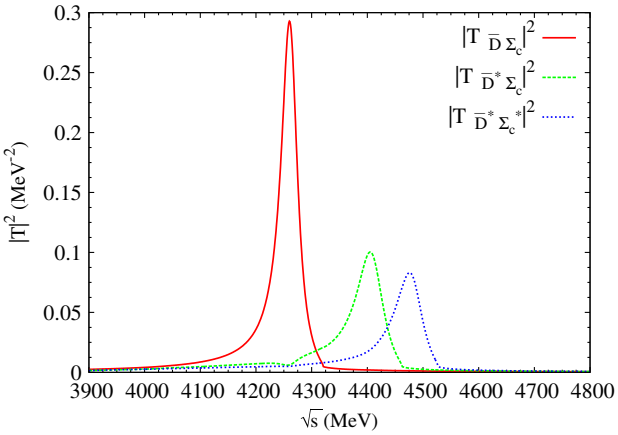

FIG. 8 (color online). The squared amplitudes of the $J = 1/2$, $I = 1/2$ sector.

nonzero width, we look for the poles corresponding to these peaks in the second Riemann sheet and find the poles at $(4261.87 + i17.84)$ MeV, $(4410.13 + i29.44)$ MeV, $(4481.35 + i28.91)$ MeV. The couplings to the various coupled channels for these poles are given in Table I. From Table I we can see that the first pole, $(4261.87 + i17.84)$ MeV, couples mostly to $\bar{D}\Sigma_c$. It could be considered a $\bar{D}\Sigma_c$ bound state that, however, decays into the open channels $\eta_c N$ and $J/\psi N$. The $\bar{D}\Sigma_c$ threshold is at 4320.8 MeV and, thus, the $\bar{D}\Sigma_c$ state is bound by about 58 MeV. The second pole couples most strongly to $\bar{D}^*\Sigma_c$. In this channel the threshold is 4462.2 MeV, and thus we have a state bound by about 52 MeV, much in line with what one expects from heavy quark symmetry comparing this with the former state. This state decays mostly into the $\eta_c N$ and $J/\psi N$ channels again. These two states correspond to those reported in [1,2], and also the first one, the $\bar{D}\Sigma_c$ state, is consistent with the results using different models [73,74]. In our work, we obtain one more new baryon state, $(4481.35 + i28.91)$ MeV, with total momentum $J = 1/2$, which couples mostly to $\bar{D}^*\Sigma_c^*$. Since in [1,2] one did not include the baryons of $J^P = 3/2^+$, their consideration here leads to a new resonance. The threshold for the $\bar{D}^*\Sigma_c^*$ channel is 4526.7 MeV and, hence, the state can be considered as a $\bar{D}^*\Sigma_c^*$ bound state by about 46 MeV, which decays mostly in $\eta_c N$ and $J/\psi N$.

For the $J = 3/2, I = 1/2$ sector, we show our results in Fig. 9. From the results of $|T|^2$, we can also see three clear peaks around the range 4300–4500 MeV, which are not far below the thresholds of $\bar{D}\Sigma_c^*$, $\bar{D}^*\Sigma_c$, $\bar{D}^*\Sigma_c^*$, respectively. The strength of the second peak is 17 times bigger than the other two, and the widths are small enough to allow the peaks to show up clearly. We have also checked that in these channels the real parts of the propagator G, Eq. (64), are acceptable too. So, these are our predictions for the new baryon states with total momentum $J = 3/2$. We search the poles in the second Riemann sheet and

TABLE I. The coupling constants of all channels corresponding to certain poles in the $J = 1/2$, $I = 1/2$ sector.

$4261.87 + i17.84$	$\eta_c N$	$J/\psi N$	$\bar{D}\Lambda_c$	$\bar{D}\Sigma_c$	$\bar{D}^*\Lambda_c$	$\bar{D}^*\Sigma_c$	$\bar{D}^*\Sigma_c^*$
g_i	$1.04 + i0.05$	$0.76 - i0.08$	$0.02 - i0.02$	$3.12 - i0.25$	$0.14 - i0.48$	$0.33 - i0.68$	$0.16 - i0.28$
$\lvert g_i\rvert$	1.05	0.76	0.02	3.13	0.50	0.75	0.32
$4410.13 + i29.44$	$\eta_c N$	$J/\psi N$	$\bar{D}\Lambda_c$	$\bar{D}\Sigma_c$	$\bar{D}^*\Lambda_c$	$\bar{D}^*\Sigma_c$	$\bar{D}^*\Sigma_c^*$
g_i	$0.34 + i0.16$	$1.43 - 0.12$	$0.15 - i0.10$	$0.20 - i0.05$	$0.17 - i0.11$	$3.05 - i0.54$	$0.07 - i0.51$
$\lvert g_i\rvert$	0.38	1.44	0.18	0.20	0.20	3.10	0.51
$4481.35 + i28.91$	$\eta_c N$	$J/\psi N$	$\bar{D}\Lambda_c$	$\bar{D}\Sigma_c$	$\bar{D}^*\Lambda_c$	$\bar{D}^*\Sigma_c$	$\bar{D}^*\Sigma_c^*$
g_i	$1.15 - i0.04$	$0.72 + i0.03$	$0.18 - i0.08$	$0.10 - i0.03$	$0.09 - i0.08$	$0.09 - i0.06$	$2.88 - i0.57$
$\lvert g_i\rvert$	1.15	0.72	0.19	0.10	0.12	0.11	2.93

TABLE II. The coupling constants to various channels for certain poles in the $J = 3/2$, $I = 1/2$ sector.

$4334.45 + i19.41$	$J/\psi N$	$\bar{D}^*\Lambda_c$	$\bar{D}^*\Sigma_c$	$\bar{D}\Sigma_c^*$	$\bar{D}^*\Sigma_c^*$
g_i	$1.31 - i0.18$	$0.16 - i0.23$	$0.20 - i0.48$	$2.97 - i0.36$	$0.24 - i0.76$
$\lvert g_i\rvert$	1.32	0.28	0.52	2.99	0.80
$4417.04 + i4.11$	$J/\psi N$	$\bar{D}^*\Lambda_c$	$\bar{D}^*\Sigma_c$	$\bar{D}\Sigma_c^*$	$\bar{D}^*\Sigma_c^*$
g_i	$0.53 - i0.07$	$0.08 - i0.07$	$2.81 - i0.07$	$0.12 - i0.10$	$0.11 - i0.51$
$\lvert g_i\rvert$	0.53	0.11	2.81	0.16	0.52
$4481.04 + i17.38$	$J/\psi N$	$\bar{D}^*\Lambda_c$	$\bar{D}^*\Sigma_c$	$\bar{D}\Sigma_c^*$	$\bar{D}^*\Sigma_c^*$
g_i	$1.05 + i0.10$	$0.18 - i0.09$	$0.12 - i0.10$	$0.22 - i0.05$	$2.84 - i0.34$
$\lvert g_i\rvert$	1.05	0.20	0.16	0.22	2.86

find $(4334.45 + i19.41)$ MeV, $(4417.04 + i4.11)$ MeV, $(4481.04 + i17.38)$ MeV. The couplings to each coupled channel corresponding to these poles are listed in Table II. From Table II, we find that the first pole, $(4334.45 + i19.41)$ MeV, couples most strongly to the channel $\bar{D}\Sigma_c^*$ and corresponds to a $\bar{D}\Sigma_c^*$ state, bound by 51 MeV with respect to its threshold of 4385.3 MeV, decaying essentially into $J/\psi N$. The state corresponding to the big peak in Fig. 9 (left) couples mostly to $\bar{D}^*\Sigma_c$; it is bound by 45 MeV with respect to the threshold of this channel, 4462.2 MeV, and decays mostly into $J/\psi N$. The third state with $J = 3/2, I = 1/2$ couples mostly to $\bar{D}^*\Sigma_c^*$, is bound by 45 MeV with respect to the threshold of this channel, 4526.7 MeV and also decays mostly into $J/\psi N$.

Finally, we also find a new bound state of $\bar{D}^*\Sigma_c^*$ around $(4487.10 + i0)$ MeV in the $J = 5/2$, $I = 1/2$ sector, as

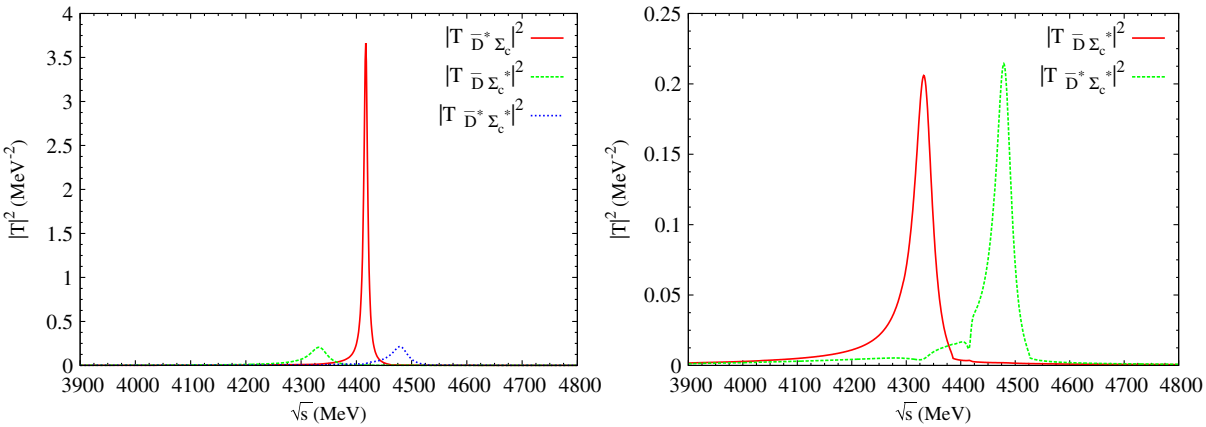

FIG. 9 (color online). The results of $|T|^2$ for the $J = 3/2$, $I = 1/2$ sector. The right panels shows the two small peaks of the left figure magnified.

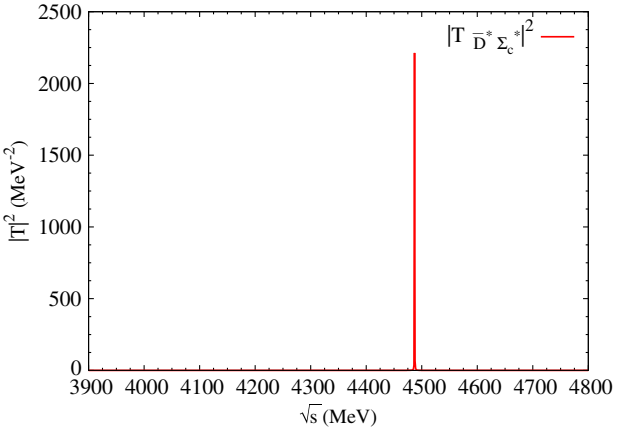

FIG. 10 (color online). The results of $|T|^2$ for the $J = 5/2$, $I = 1/2$ sector.

shown in Fig. 10. As we can see in the figure, the state has no width, as it corresponds to a single channel, $\bar{D}^*\Sigma_c^*$ of Eq. (33). It is then a bound state in this channel. The pole appears in the first Riemann sheet, and the state is bound by about 40 MeV with respect to the $\bar{D}^*\Sigma_c^*$ threshold.

The states that we have reported are different states since they correspond to different energies or different total spin J. Hence, we obtain seven states. Yet, we find that some states of a given meson and baryon appear at about the same energy but different J. This is to be expected from the hidden gauge dynamics because for $\bar{D}^*B$ the main diagonal terms have an interaction of the type $\vec{\epsilon}\vec{\epsilon}'$, which is spin independent. Then, up to the small mixing with other channels, we get states degenerate in $J = 1/2, 3/2$ for $\bar{D}^*\Sigma_c$ and $J = 1/2, 3/2, 5/2$ for $\bar{D}^*\Sigma_c^*$. From this perspective we can present our results by saying that we get four states bound by about 40–50 MeV, corresponding to $\bar{D}\Sigma_c$, $\bar{D}\Sigma_c^*$ with $J = 1/2, 3/2$, respectively, $\bar{D}^*\Sigma_c$ degenerated with $J = 1/2, 3/2$, and $\bar{D}^*\Sigma_c^*$ degenerated with $J = 1/2, 3/2, 5/2$.

The results reported in [47] show a certain parallelism with those found here. There, seven odd-parity N-like states were also found (three with spins $1/2$ and $3/2$ and a further one with spin $5/2$). Moreover, the dynamics of these resonances is strongly influenced by the $\bar{D}^{(*)}\Sigma_c^{(*)}$ components, as is the case here. Their masses, however, are quite different since those found in [47] lie in the region of 4 GeV, thus being significantly lighter than those found in this work. Besides differences of dynamical origin [SU(8) extension of the WT interaction + pattern of spin-flavor symmetry breaking versus SU(4) extension of the hidden gauge approach + pattern of flavor symmetry breaking] that can help us to understand these changes in the position of the masses, there exists a major difference among both approaches in what concerns the renormalization of the loop function $G(s)$ in the coupled channels space. The baryon-meson propagator is logarithmically ultraviolet divergent; thus, the loop needs to be renormalized. Here, we use Eq. (64) with a scale $\mu = 1000$ MeV, and the subtraction constant $a(\mu)$ is set to -2.3, as it was done in [1,2]. However, in [47] a subtraction point regularization is chosen such that $G_{ii}(s) = 0$ at a certain point $\sqrt{s} = \mu_I$. The subtraction point μ_I is set to $\sqrt{m_{\rm th}^2 + M_{\rm th}^2}$, where $m_{\rm th}$ and $M_{\rm th}$ are, respectively, the masses of the meson and baryon producing the lowest threshold (minimal value of $m_{\rm th} + M_{\rm th}$) for each I (isospin) sector, independent of the angular momentum J. This renormalization scheme was first proposed in Refs. [33,34], and it was successfully used in Refs. [75,76] for three light flavors and in the open charm (bottom) studies carried out in [44–46] (also [48]). Both renormalization schemes (the one used in this work and that employed in [47]) lead to similar results for the case of light flavors but, however, produce quite different results in the hidden-charm sector studied here. Indeed, a significant part of the differences between the masses of the resonances found here and those reported in [47] can be attributed to the different renormalization procedure followed in both works. As an example, let look at the $I = 1/2$, $J = 5/2$ sector, where there is only one coupled channel: $\bar{D}^*\Sigma_c^*$. The interactions used here and in Ref. [47] are attractive and nearly the same, once we take into account that for this particular channel $1/f^2$ is replaced by $1/f_{D^*}^2$ in [47] according to the pattern of spin-flavor symmetry breaking implemented in that work (see Sec. IIIB of [47]). However, the state found in [47] is around 450 MeV lighter (more bound) than that predicted here. This difference can only be attributed to the renormalization scheme.[2] Large binding energies cannot be discarded. For instance, interpreting the $\Lambda_c(2595)$ in the open charm sector as a $\bar{D}^*N$ bound state [44,46] would lead to a binding energy of around 350 MeV. On the other hand, the subtraction constant (main difference of the two renormalization schemes) generates terms at the next order of the expansion used to determine the potential [66]. Thus, different values for the subtraction constant can only be discriminated with the help of some phenomenological input, for instance, the position of some states, which could be used to constrain such terms.

We would like to finish this discussion by just stressing again that, ignoring the difference in the mass positions, the isospin $1/2$ states found in this work have a clear resemblance with those reported in [47]. The predicted new resonances definitely cannot be accommodated by quark models with three constituent quarks, and they might be looked for in the forthcoming PANDA experiment at the future FAIR facility.

[2]We should note that in [47], the interaction is split into different irreducible representations of the symmetry group, and only those sectors where the interaction is attractive are studied.

VII. CONSIDERATIONS ON HQSS AND SU(4) SYMMETRY BREAKING

The results obtained in the former sections rely upon exact HQSS and SU(4) symmetries. We expect some breaking of these symmetries, and we study uncertainties of the results tied to these sources.

SU(4) symmetry is expected to be broken in a much larger amount than SU(3). Yet, when one talks about SU(3) or SU(4) breaking, one must be more specific about what magnitude one is talking about. The different masses of the quarks or mesons and baryons associated with the group multiplets are largely responsible for the symmetry breaking of some magnitudes. There is a clear example of a large SU(3) breaking that is tied to the unitarization and not to elementary vertices: The chiral Lagrangians used in the study of the strangeness $S = -1$ sector in the pseudoscalar-baryon interaction are SU(3) symmetric. Upon unitarization in coupled channels and taking equal masses for the baryons of the octet of the nucleon and the mesons of the octet of the pion, one obtains a meson-baryon bound state as an octet and another one as a singlet of the SU(3). When the masses in the two octets are taken as the physical ones, the octet splits into two branches and the singlet changes position [75,77]. One of the two octets becomes the $\Lambda(1670)$ while the other one gives rise to the second $\Lambda(1405)$ pole at 1420 MeV. The coupled channels rescattering using physical masses has been responsible for a shift of 250 MeV into two states which are degenerate in an SU(3) symmetric world. Yet, the chiral Lagrangian itself is SU(3) invariant. This example tells us that the SU(3) [or SU(4)] symmetry should be assumed in elementary vertices where the masses do not play a role, while one should be ready to accept large breaking in some physical magnitudes where the different scales in the masses are bound to have an effect. A further discussion along these lines can be seen in Sec. II.D of [2], and uncertainties related to SU(4) breaking are also discussed in Sec. V of [78].

Contrary to some expectations that SU(4) symmetry should be badly broken, when applied to elementary couplings it works better than expected, as one can see in radiative decays and associated processes [79].

But we want to be more specific here, and we concentrate on the vertices that appear in our theory. In the local hidden gauge approach the leading term in the meson-baryon interaction is provided by the mechanism of Fig. 2, exchanging light vector mesons. We will concentrate on the $DD\rho$ vertex for which there are evaluations using the Dyson-Schwinger equation [80] and QCD lattice gauge simulations [81]. The coupling $g_{DD\rho}$ is obtained in [80] with the value $g_{DD\rho} \simeq 5$ and in [81] with the value $g_{DD\rho} \simeq 4.9$, which contrasts with the SU(4) value of $g_{DD\rho} = g_{KK\rho} \simeq 2$ obtained in [38]. In principle, one does not need SU(4) to obtain this value as long as the c quarks in $g_{DD\rho}$ and s quarks in $g_{KK\rho}$ act as spectators. Hence, one would get this equality in the couplings, which means that with the assumption of the c quarks being spectators one can get the $g_{DD\rho}$ coupling from $g_{\pi\pi\rho}$ using simply SU(3). From this perspective, we can say that the results of Refs. [80,81] challenge the spectator hypothesis.

One might think that the use of this new coupling, considerably increasing the strength of the potential, will drastically change the results obtained. One can guess that changes would not be so drastic because, simultaneously with this large coupling, a form factor arises, and one has an effective coupling

$$F_{DD\rho}(\vec{q}^2) \equiv g_{DD\rho}\tilde{F}(\vec{q}^2), \qquad \tilde{F}(\vec{q}^2) = \frac{\Lambda^2}{\Lambda^2 + \vec{q}^2}, \quad (67)$$

with $\Lambda \simeq 0.7$ GeV, which softens the interaction in the loops. Actually, the integrated interaction (propagator times squared form factor) in [80] is only 40% larger than in [38], where the equivalent Λ is 1.4 GeV. This integrated interaction is about 20% larger than that of [82]. We can actually see the effects of such new couplings in the binding energy in our problem. For this purpose we choose one of the cases $J = 1/2$, $I = 1/2$ (for the other cases the effects are similar). Then, following [83], we change the present formalism a bit to incorporate the form factor $\tilde{F}(\vec{q}^2)$ of Eq. (67). We assume that the lower vertex $BB\rho$ does not change with respect to the one we have. This exercise is sufficient to get a sense of the uncertainties that we have for adhering to SU(3) or SU(4) symmetry. Then we use Eq. (47) to obtain the $\tilde{T}$ matrix but, according to [83], now we have

$$\begin{aligned} V \to \tilde{V} &\equiv \frac{g_{DD\rho}(new)}{g_{DD\rho}(SU(4))} V, \\ G \to \tilde{G} &= \int \frac{d^3\vec{q}}{(2\pi)^3} \tilde{F}^2(\vec{q}^2) \frac{\omega_P + \omega_B}{2\omega_P\omega_B} \\ &\quad \times \frac{2M_B}{P^{02} - (\omega_P + \omega_B)^2 + i\varepsilon}, \end{aligned} \quad (68)$$

with ω_P, ω_B, M_B, P^0 the relativistic energy of the pseudoscalar, the baryon, the mass of the baryon, and the total energy of the system, respectively. Equation (68) incorporates the form factor $\tilde{F}^2(\vec{q}^2)$ into the usual integrand of the G function. To implement the form factor we have to use an explicit momentum integration for $\tilde{G}$ in Eq. (68), instead of the dimensional regularization formula used so far. For this purpose we first find the cutoff $q_{\max}$ in the integration, such that the results are similar to those found with dimensional regularization. This $q_{\max}$ is found around $q_{\max} = 820$ MeV, similar to what was used in [1,2].

The results with the modified potential can be seen in Fig. 11, compared to those obtained using $q_{\max} = 820$ MeV with no modification of the potential [this is obtained using $\tilde{G}$ in Eq. (68) with $\tilde{F}(\vec{q}^2) = 1$]. The same three peaks in $|T|^2$ appear now, albeit with different

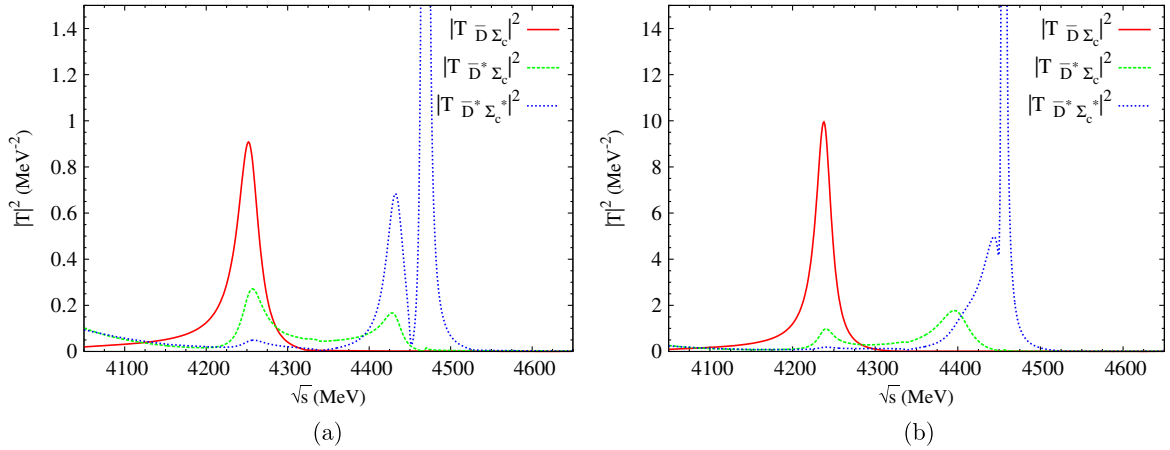

FIG. 11 (color online). The results of squared amplitudes for the $J = 1/2$, $I = 1/2$ sector: (a) With $q_{\max} = 820$ MeV; (b) with $q_{\max} = 820$ MeV but with the modified potential of Eq. (68).

strength and at different energies. Since our only concern is to see if there are bound states and to obtain an estimate on the binding energy, we can see that this is indeed the case, and the binding energies are changed but within the same order of magnitude.

We now make more comments about Fig. 11. If we compare the results obtained with the cutoff method with $q_{\max} = 820$ MeV with those of the dimensional regularization of Fig. 8, we can see that the lower and higher peaks have both changed by about 12 MeV. The middle one has changed by a similar amount but in the opposite direction (this is a consequence of the interference of coupled channels). What we see is that we have differences of $\pm$(10–15) MeV in the bindings from using different regularization methods on the loop function. We must accept these as systematic uncertainties of our approach.

If we now compare panels (a) and (b) in Fig. 11, we can see that the effect of using the increased $g_{DD\rho}$ coupling and the form factor simultaneously is an increase of the binding by 12–14 MeV for the lower and upper states (the small side structure in the upper peak comes from a numerical artifact with no physical meaning), and the middle one is shifted by 36 MeV, but compared to the results of dimensional regularization by 21 MeV. The changes obtained from this source are of the same order of magnitude as changes from using two different regularization methods.

The other issue we want to discuss is the effect on the breaking of the HQSS. HQSS is an exact symmetry of QCD in the limit of infinitely heavy quarks, the question is how relevant numerically can be the subleading corrections, terms of $\mathcal{O}(m_Q^0)$ in the potential in our formalism. One estimate can be provided by the relevance of the contact terms in the vector-vector interaction in the local hidden gauge approach. These terms are indeed one order lower in m_Q in the potential and hence

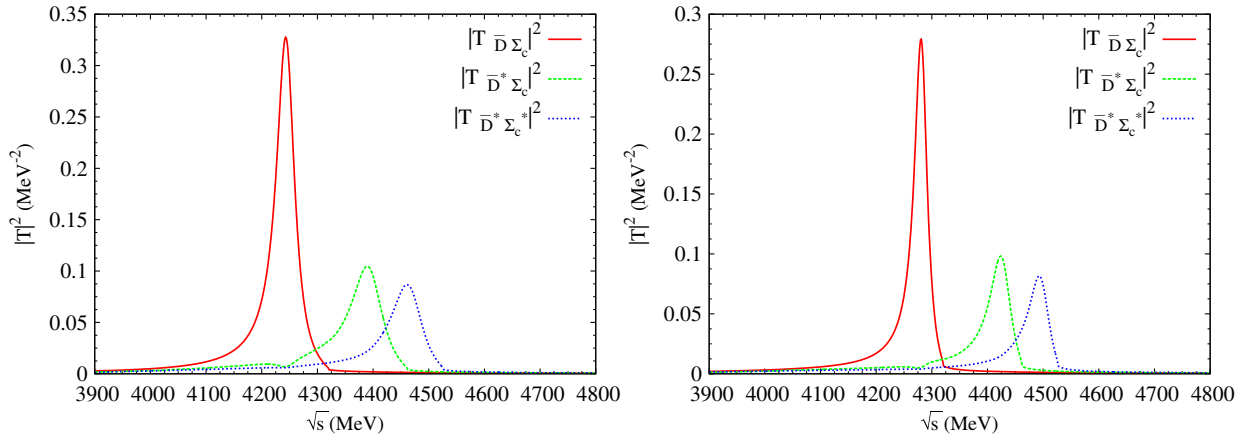

FIG. 12 (color online). The results of squared amplitudes for the $J = 1/2$, $I = 1/2$ sector, which have a modified factor in the potentials. Left panel: $1.20 \times V$; right panel: $0.80 \times V$.

subdominant. Yet, numerically they correspond to corrections of the order of 20% in the charm sector. In the beauty sector the corrections are much smaller, and HQSS is assumed to be very accurate there. The 20% violation of this symmetry in the charm sector is in line with findings in lattice QCD, or the Dyson-Schwinger equation. Indeed, in [81] it is found that $g_{DD\rho} \simeq 4.90$ while $g_{D^*D^*\rho} \simeq 5.42$. Similar breakings are found in the D or D^* decay constants (f_D, f_{D^*}) in [84] from QCD lattice gauge calculations, comparing g_{D_sDK} and g_{B_sBK} in [85], evaluated with the Dyson-Schwinger equations, in the QCD lattice evaluation of the D^{*0} magnetic moment [86], or in the QCD sum rule evaluation of the $DD\rho$ and $D^*D^*\rho$ couplings [87].

In view of these findings we perform an exercise similar to the former one, evaluating the T matrix with the interaction used in the former section multiplied by 1.20 or 0.80, respectively. The results can be seen in Fig. 12 for $J = 1/2$, $I = 1/2$. We can see that, with respect to the results with weight unity in the potential, the results with $1.20 \times V$ lead to a binding increased by about 15 MeV, while those with $0.80 \times V$ produce smaller bindings, with energies shifted by about 20 MeV. The former exercises have shown that the changes produced by using different couplings obtained in other approaches to QCD, with a certain amount of SU(4) or HQSS breaking, induce changes of the order of 20–30 MeV in bindings estimated in our approach to be of the order of 50 MeV. These uncertainties are in line with other systematic uncertainties that we must also admit from our partial ignorance in the regularization scale of the loops. Yet, with all these uncertainties, the binding of the states remains a solid conclusion, as does the order of magnitude of the binding energies; the maximum one can hope without further experimental information to constrain the input in our theory.

VIII. CONCLUSIONS

In this paper we have addressed a relevant topic, which is to show the consistency of the dynamics of the local hidden gauge Lagrangians extrapolated to SU(4) with the LO constraints of heavy quark spin symmetry. These latter constraints are very powerful since they have their roots in the QCD Lagrangian and must be understood as very stringent. To show the consistency we have addressed the problem of the interaction of mesons and baryons with hidden charm, a problem of much current interest in view of ongoing work at the BES, BELLE, FAIR and other facilities. Once again, the requirements of HQSS demanded that we put together pseudoscalar and vector mesons, as well as baryons with $J = 1/2, 3/2$. A series of relationships were developed for the transition potentials between the different meson-baryon channels in different combinations of spin and isospin. After this, we evaluated these matrix elements using the dynamics of the local hidden gauge approach and found them to fulfill all the relationships of LO HQSS while at the same time providing some determined expressions for them, which allowed us to find out about the existence of several bound states or resonances stemming from this interaction. We found seven states with different energies or different spin-isospin quantum numbers. Yet, the fact that the interaction that we had for vector-baryon factorizes as $\epsilon \cdot \epsilon'$ produces matrix elements which are degenerate in the different spins allowed by the meson-baryon combinations. Hence, up to some different mixing with subleading channels, we found a very approximate degeneracy in the states that qualify as quasibound $\bar{D}^*B$. In view of this, the seven states that we found could be more easily classified as four basic states corresponding to a quasibound $\bar{D}\Sigma_c$ state that appears in $J = 1/2$, a $\bar{D}\Sigma_c^*$ state in $J = 3/2$, a $\bar{D}^*\Sigma_c$ state that appears nearly degenerate in $J = 1/2, 3/2$, and a $\bar{D}^*\Sigma_c^*$ state that appears nearly degenerate in $J = 1/2, 3/2, 5/2$. All the states are bound with about 50 MeV with respect to the corresponding $\bar{D}B$ thresholds, and the width, except for the $J = 5/2$ state, is also of the same order of magnitude. The $J = 5/2$ state that appears in the single $\bar{D}^*\Sigma_c^*$ channel has the peculiarity that it has zero width in the space of states chosen. All the states found appear in $I = 1/2$, and we found no states in $I = 3/2$. We have also made some effort estimating uncertainties from the breaking of SU(4) and HQSS. While they indeed introduce changes in the binding energies, the results in the appearance of the bound states are stable under these changes, as is the order of magnitude of the binding, with binding energies that can increase by 30%–50%.

The masses obtained here are substantially heavier than those found in another model [47] that also fulfills HQSS, but incorporates some elements of extra SU(8) symmetry and a different renormalization scheme. In spite of this, the latter model also predicts the same J^P quantum numbers for these states. Experiments that search for the states predicted will bring further light on this issue in the future.

ACKNOWLEDGMENTS

C. W. X. thanks C. Hanhart, F. K. Guo, W. H. Liang, K. U. Can, A. Ozpineci, and L. L. Salcedo for helpful discussions. This work is partly supported by the Spanish Ministerio de Economia y Competitividad and European FEDER funds under Contracts No. FIS2011-28853-C02-01 and No. FIS2011-28853-C02-02, and the Generalitat Valenciana in the program Prometeo, 2009/090. We acknowledge the support of the European Community-Research Infrastructure Integrating Activity Study of Strongly Interacting Matter (Hadron Physics 3, Grant No. 283286) under the Seventh Framework Programme of the EU.

[1] J.-J. Wu, R. Molina, E. Oset, and B. S. Zou, Phys. Rev. Lett. **105**, 232001 (2010).
[2] J.-J. Wu, R. Molina, E. Oset, and B. S. Zou, Phys. Rev. C **84**, 015202 (2011).
[3] M. Bando, T. Kugo, S. Uehara, K. Yamawaki, and T. Yanagida, Phys. Rev. Lett. **54**, 1215 (1985).
[4] M. Bando, T. Kugo, and K. Yamawaki, Phys. Rep. **164**, 217 (1988).
[5] U. G. Meissner, Phys. Rep. **161**, 213 (1988).
[6] S. Weinberg, Physica (Amsterdam) **96**, 327 (1979).
[7] J. Gasser and H. Leutwyler, Ann. Phys. (N.Y.) **158**, 142 (1984).
[8] J. J. Sakurai, *Currents and Mesons* (University of Chicago, Chicago, 1969).
[9] G. Ecker, J. Gasser, H. Leutwyler, A. Pich, and E. de Rafael, Phys. Lett. B **223**, 425 (1989).
[10] R. Molina, D. Nicmorus, and E. Oset, Phys. Rev. D **78**, 114018 (2008).
[11] L. S. Geng and E. Oset, Phys. Rev. D **79**, 074009 (2009).
[12] H. Nagahiro, J. Yamagata-Sekihara, E. Oset, S. Hirenzaki, and R. Molina, Phys. Rev. D **79**, 114023 (2009).
[13] T. Branz, L. S. Geng, and E. Oset, Phys. Rev. D **81**, 054037 (2010).
[14] A. Martinez Torres, L. S. Geng, L. R. Dai, B. X. Sun, E. Oset, and B. S. Zou, Phys. Lett. B **680**, 310 (2009).
[15] L. S. Geng, F. K. Guo, C. Hanhart, R. Molina, E. Oset, and B. S. Zou, Eur. Phys. J. A **44**, 305 (2010).
[16] R. Molina, H. Nagahiro, A. Hosaka, and E. Oset, Phys. Rev. D **80**, 014025 (2009).
[17] R. Molina and E. Oset, Phys. Rev. D **80**, 114013 (2009).
[18] R. Molina, T. Branz, and E. Oset, Phys. Rev. D **82**, 014010 (2010).
[19] Y. Dong, A. Faessler, T. Gutsche, and V. E. Lyubovitskij, J. Phys. G **40**, 015002 (2013).
[20] T. Branz, T. Gutsche, and V. E. Lyubovitskij, Phys. Rev. D **82**, 054010 (2010).
[21] T. Branz, T. Gutsche, and V. E. Lyubovitskij, Phys. Rev. D **82**, 054025 (2010).
[22] I. W. Lee, A. Faessler, T. Gutsche, and V. E. Lyubovitskij, Phys. Rev. D **80**, 094005 (2009).
[23] S. Sarkar, B.-X. Sun, E. Oset, and M. J. Vicente Vacas, Eur. Phys. J. A **44**, 431 (2010).
[24] E. Oset and A. Ramos, Eur. Phys. J. A **44**, 445 (2010).
[25] J. Beringer *et al.* (Particle Data Group Collaboration), Phys. Rev. D **86**, 010001 (2012).
[26] E. J. Garzon and E. Oset, Eur. Phys. J. A **48**, 5 (2012).
[27] K. P. Khemchandani, H. Kaneko, H. Nagahiro, and A. Hosaka, Phys. Rev. D **83**, 114041 (2011).
[28] K. P. Khemchandani, A. Martinez Torres, H. Kaneko, H. Nagahiro, and A. Hosaka, Phys. Rev. D **84**, 094018 (2011).
[29] K. P. Khemchandani, A. Martinez Torres, H. Nagahiro, and A. Hosaka, Phys. Rev. D **85**, 114020 (2012).
[30] E. Oset, A. Ramos, E. J. Garzon, R. Molina, L. Tolos, C. W. Xiao, J. J. Wu, and B. S. Zou, Int. J. Mod. Phys. E **21**, 1230011 (2012).
[31] M. F. M. Lutz and E. E. Kolomeitsev, Nucl. Phys. **A730**, 110 (2004).
[32] M. F. M. Lutz and E. E. Kolomeitsev, Nucl. Phys. **A755**, 29 (2005).
[33] J. Hofmann and M. F. M. Lutz, Nucl. Phys. **A763**, 90 (2005).
[34] J. Hofmann and M. F. M. Lutz, Nucl. Phys. **A776**, 17 (2006).
[35] L. Tolos, J. Schaffner-Bielich, and A. Mishra, Phys. Rev. C **70**, 025203 (2004).
[36] T. Mizutani and A. Ramos, Phys. Rev. C **74**, 065201 (2006).
[37] C. E. Jimenez-Tejero, A. Ramos, and I. Vidana, Phys. Rev. C **80**, 055206 (2009).
[38] J. Haidenbauer, G. Krein, U.-G. Meissner, and A. Sibirtsev, Eur. Phys. J. A **33**, 107 (2007).
[39] J. Haidenbauer, G. Krein, U.-G. Meissner, and A. Sibirtsev, Eur. Phys. J. A **37**, 55 (2008).
[40] J. Haidenbauer, G. Krein, U.-G. Meissner, and L. Tolos, Eur. Phys. J. A **47**, 18 (2011).
[41] N. Isgur and M. B. Wise, Phys. Lett. B **232**, 113 (1989).
[42] M. Neubert, Phys. Rep. **245**, 259 (1994).
[43] A. V. Manohar and M. B. Wise, *Heavy Quark Physics*, Cambridge Monographs on Particle Physics, Nuclear Physics and Cosmology Vol. 10 (Cambridge University Press, Cambridge, England, 2000).
[44] C. Garcia-Recio, V. K. Magas, T. Mizutani, J. Nieves, A. Ramos, L. L. Salcedo, and L. Tolos, Phys. Rev. D **79**, 054004 (2009).
[45] D. Gamermann, C. Garcia-Recio, J. Nieves, L. L. Salcedo, and L. Tolos, Phys. Rev. D **81**, 094016 (2010).
[46] O. Romanets, L. Tolos, C. Garcia-Recio, J. Nieves, L. L. Salcedo, and R. G. E. Timmermans, Phys. Rev. D **85**, 114032 (2012).
[47] C. Garcia-Recio, J. Nieves, O. Romanets, L. L. Salcedo, and L. Tolos, Phys. Rev. D **87**, 074034 (2013).
[48] C. Garcia-Recio, J. Nieves, O. Romanets, L. L. Salcedo, and L. Tolos, Phys. Rev. D **87**, 034032 (2013).
[49] R. Aaij *et al.* (LHCb Collaboration), Phys. Rev. Lett. **109**, 172003 (2012).
[50] J. Nieves and M. P. Valderrama, Phys. Rev. D **86**, 056004 (2012).
[51] C. Hidalgo-Duque, J. Nieves, and M. P. Valderrama, Phys. Rev. D **87**, 076006 (2013).
[52] C. Hidalgo-Duque, J. Nieves, and M. P. Valderrama, arXiv:1211.7004.
[53] F.-K. Guo, C. Hanhart, and U.-G. Meissner, Phys. Rev. Lett. **102**, 242004 (2009).
[54] F.-K. Guo, C. Hidalgo-Duque, J. Nieves, and M. P. Valderrama, arXiv:1303.6608.
[55] M. E. Rose, *Elementary Theory of Angular Momentum* (John Wiley, New York, 1957).
[56] H. Nagahiro, L. Roca, A. Hosaka, and E. Oset, Phys. Rev. D **79**, 014015 (2009).
[57] D. Gamermann, E. Oset, and B. S. Zou, Eur. Phys. J. A **41**, 85 (2009).
[58] F. Klingl, N. Kaiser, and W. Weise, Nucl. Phys. **A624**, 527 (1997).
[59] J. E. Palomar and E. Oset, Nucl. Phys. **A716**, 169 (2003).
[60] G. Ecker, Prog. Part. Nucl. Phys. **35**, 1 (1995).
[61] V. Bernard, N. Kaiser, and U. G. Meissner, Int. J. Mod. Phys. E **04**, 193 (1995).
[62] E. E. Jenkins and A. V. Manohar, Phys. Lett. B **259**, 353 (1991).
[63] F. E. Close, *An Introduction to Quarks and Partons* (Academic Press, London, 1979).
[64] E. Oset and A. Ramos, Nucl. Phys. **A635**, 99 (1998).

[65] J. A. Oller and U. G. Meissner, Phys. Lett. B **500**, 263 (2001).
[66] J. Nieves and E. Ruiz Arriola, Nucl. Phys. **A679**, 57 (2000).
[67] B. Borasoy, Phys. Rev. D **59**, 054021 (1999).
[68] D. Gamermann, J. Nieves, E. Oset, and E. Ruiz Arriola, Phys. Rev. D **81**, 014029 (2010).
[69] J.-J. Wu and B. S. Zou, Phys. Lett. B **709**, 70 (2012).
[70] F.-K. Guo, R.-G. Ping, P.-N. Shen, H.-C. Chiang, and B.-S. Zou, Nucl. Phys. **A773**, 78 (2006).
[71] L. Roca, E. Oset, and J. Singh, Phys. Rev. D **72**, 014002 (2005).
[72] J. Yamagata-Sekihara, J. Nieves, and E. Oset, Phys. Rev. D **83**, 014003 (2011).
[73] J.-J. Wu, T.-S. H. Lee, and B. S. Zou, Phys. Rev. C **85**, 044002 (2012).
[74] W. L. Wang, F. Huang, Z. Y. Zhang, and B. S. Zou, Phys. Rev. C **84**, 015203 (2011).
[75] C. Garcia-Recio, M. F. M. Lutz, and J. Nieves, Phys. Lett. B **582**, 49 (2004) .
[76] D. Gamermann, C. Garcia-Recio, J. Nieves, and L. L. Salcedo, Phys. Rev. D **84**, 056017 (2011).
[77] D. Jido, J. A. Oller, E. Oset, A. Ramos, and U. G. Meissner, Nucl. Phys. **A725**, 181 (2003).
[78] R. Molina, H. Nagahiro, A. Hosaka, and E. Oset, Phys. Rev. D **80**, 014025 (2009).
[79] D. Gamermann, Ph.D. thesis, University of Valencia, 2010, http://ific.uv.es/nucth/tesis_DanGam.pdf.
[80] B. El-Bennich, G. Krein, L. Chang, C. D. Roberts, and D. J. Wilson, Phys. Rev. D **85**, 031502 (2012).
[81] K. U. Can, G. Erkol, M. Oka, A. Ozpineci, and T. T. Takahashi, Phys. Lett. B **719**, 103 (2013).
[82] Y. Yamaguchi, S. Ohkoda, S. Yasui, and A. Hosaka, Phys. Rev. D **84**, 014032 (2011).
[83] F. Aceti and E. Oset, Phys. Rev. D **86**, 014012 (2012).
[84] D. Becirevic, V. Lubicz, F. Sanfilippo, S. Simula, and C. Tarantino, J. High Energy Phys. 02 (2012) 042.
[85] B. El-Bennich, C. D. Roberts, and M. A. Ivanov, arXiv:1202.0454.
[86] D. Becirevic and B. Haas, Eur. Phys. J. C **71**, 1734 (2011).
[87] M. E. Bracco, M. Chiapparini, F. S. Navarra, and M. Nielsen, Prog. Part. Nucl. Phys. **67**, 1019 (2012).